AD-A128 289 ENERGY RELEASE AND FLUID DYNAMICS IN MULTIPHASE SYSTEMS 1/1
(U) SCIENCE APPLICATIONS INC MCLEAN VA
K KAILASANATH ET AL. MAR 83 SAI-84-122-WA
UNCLASSIFIED N00014-82-C-2037 F/G 20/4 NL

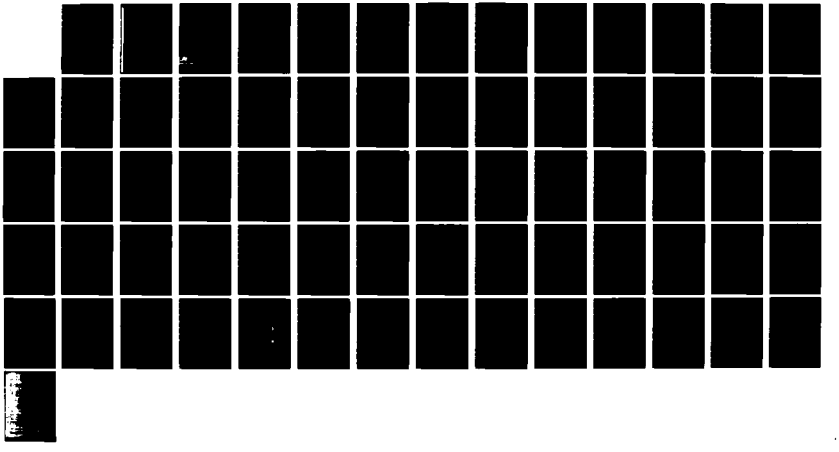

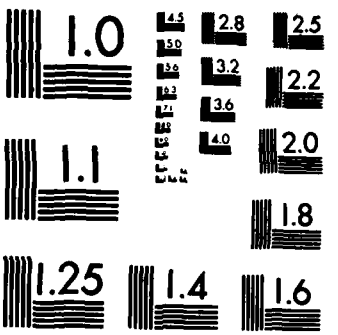

MICROCOPY RESOLUTION TEST CHART
NATIONAL BUREAU OF STANDARDS-1963-A

(12)

AD A128289

ENERGY RELEASE AND FLUID DYNAMICS IN MULTIPHASE SYSTEMS

FINAL REPORT

SAI 84-122-WA

DTIC
MAY 1 1983
E

DTIC FILE COPY

SCIENCE APPLICATIONS, INC.

This document has been approved for public release and sale; its distribution is unlimited

12

ENERGY RELEASE AND FLUID DYNAMICS IN MULTIPHASE SYSTEMS

FINAL REPORT

SAI 84-122-WA

DTIC
ELECTE
MAY 1 0 1983
S
D
E

SCIENCE APPLICATIONS, INC.
Post Office Box 1303, 1710 Goodridge Drive, McLean, Virginia 22102, (703) 821-4300

This document has been approved for public release and sale; its distribution is unlimited.

ENERGY RELEASE AND FLUID DYNAMICS IN MULTIPHASE SYSTEMS

FINAL REPORT

SAI 84-122-WA

Submitted To

Laboratory for Computational Physics
Naval Research Laboratory
Washington, D.C. 20375

Prepared Under

NRL Contract No. N00014-82-C-2037

Accession For
NTIS GRA&I
DTIC TAB
Unannounced
Justification
By
Distribution/
Availability Codes
Dist | Avail and/or Special
A

Prepared by

Kazhikathra Kailasanath
and
Ellis Hyman

March 1983

SCIENCE APPLICATIONS, INCORPORATED
1710 Goodridge Drive, McLean, VA 22102

This document has been approved for public release and sale; its distribution is unlimited.

TABLE OF CONTENTS

Page

GENERAL DISCUSSION. 1

REFERENCES. 7

APPENDIX A - Power-Energy Relations for the Direct Initiation of Detonations in Oxy-Acetylene Mixtures A-1

APPENDIX B - Numerical Simulations of Weak Ignition Behind Incident Shock Waves and the Transition to Detonation B-1

APPENDIX C - Ignition of Flamelets Behind Incident Shock Waves and the Transition to Detonation . .C-1

GENERAL DISCUSSION

In the following discussion we will summarize the work performed by Science Applications, Inc. (SAI) on "Energy Release and Fluid Dynamics in Multiphase Systems" (Contract #N00014-82-C-2037, SAI Project #1-157-18-519-00) during the technical performance period ending 7 January 1983. During this contract period, our attention was focussed primarily on (1) deriving power-energy relations for the direct initiation of detonations, and (2) ignition behind incident shocks and the transition to detonation. The efforts and accomplishments in each of these areas is described below in some detail.

Power-energy Relations for the Initiation of Detonations

Recent experimental studies[1,2,3,4] on the direct initiation of gaseous detonations have shown that initiation depends not only on the energy deposited but also on the rate at which it is deposited, namely the power. The experimental results[2] have also indicated that there is a minimum initiation energy below which a detonation will not occur no matter what the power is and that there is a minimum power below which a detonation will not occur no matter what the total energy is. The relation between the power and the energy obtained from different experimental arrangements have, however, exhibited different qualitative characteristics.

We have modified and extended a basic theoretical model proposed by Abouseif and Toong[5] and have used it to determine the relation between the power and the energy required for the initiation of planar, cylindrical and spherical detonations in a gas mixture. The model considers the generation of a constant velocity shock by means of appropriate energy addition. The flow fields behind the shocks in the three geometries are obtained by solving the one-dimensional conservation equations for mass, momentum and energy. The solution procedure is simplified by using a similarity solution. The model also requires knowledge of the duration for which the shock must be maintained in order to initiate a detonation. This time is related but not necessarily equal to the chemical induction time of the gas mixture.

The results from the model show that the qualitative differences in the power-energy relations of Dabora[4] and Knystautas and Lee[3] are due to the differences in the geometry of the detonations in the two cases. The results also show that the minimum power and the minimum energy are very sensitive to uncertainties in the ignition delay time used. Another interesting observation from the model is that the minimum power required corresponds to a shock of minimum Mach number only in the case of planar detonations. In the cylindrical and spherical cases, it is possible to

initiate a detonation with a shock wave of lower Mach number than that corresponding to the minimum power. Such a shock wave will have to be maintained for a longer time than the shock corresponding to the minimum power and hence will require a larger amount of energy.

This work will be presented at the Spring Meeting of the Western States Section of the Combustion Institute as Paper No. WSCI-83-35. A copy of this paper is included in this report as Appendix A entitled, "Power-Energy Relations for the Direct Initiation of Detonations in Oxy-Acetylene Mixtures." A more detailed account of this work is currently being prepared for publication as a NRL Memorandum Report.

An important extension of the work described above is to the study of condensed phase mixtures. For this purpose we will have to replace the perfect gas equation of state which is used in the above model with appropriate equations of state. Furthermore, instead of the induction time we need to use the run time to detonation which has been measured for several explosives[6]. With these modifications, which are currently being pursued, this theoretical model will be a valuable tool in classifying condensed phase explosives according to their sensitivity to detonations.

Ignition Behind Incident Shocks and the Transition to Detonation

Experiments[7,8,9,10] and numerical simulations[11] have shown that shock induced ignition in gaseous hydrogen-air mixtures may occur in one of two distinct modes, depending on the thermodynamic state in the shocked mixture. At lower temperatures the ignition is weak, or mild, with the gradual development of the gas dynamic explosion; at higher temperatures it is strong, or sharp, with a practically instantaneous appearance of a secondary shock induced by the explosive reaction. Furthermore, at low temperatures the formation of distinct flame kernels appears to be an essential precursor of ignition.

We have performed time-dependent numerical simulations to elucidate some of the details of weak ignition behind incident shock waves and the subsequent transition to detonation. These simulations were carried out using the NRL 1D reactive shock code[12,13] which combines a description of the fluid dynamics and detailed chemical kinetics.

The numerical simulations show that a small amount of energy released in the shocked region can be the origin of pressure waves which accelerate the shock front. This shock acceleration leads to an increase in the temperature and pressure behind it. In the weak ignition regime, a small increase in the pressure and temperature can result

in a substantial decrease in the induction time. The numerical simulations show how this leads to the formation of reaction centers. The formation of a hot spot due to energy release at one of the reaction centers and the subsequent development of a pair of reaction waves from the hot spot have been studied. The acceleration of these reaction waves into detonation waves has also been observed in the simulations.

The predictions of the model are in qualitative agreement with experimental observations. However, the model does not include multi-dimensional phenomena such as turbulence and boundary layer growth which play an important part in any quantitative study of the transition to detonation. Currently, a two-dimensional reactive shock model exists but it uses a parameterized model for energy release[14,15]. The model is now being extended to include a detailed chemical kinetic scheme. Calculations such as discussed above performed with this model will show the effects of transverse waves and boundary layers on the transition to detonation.

This work has been presented at different stages of completion both at the 35th Meeting of the American Physical Society, Division of Fluid Dynamics and at the 1982 Fall Meeting of the Eastern States Section of the Combustion Institute. A short version of these presentations is included

in this report as Appendix B entitled, "Numerical Simulations of Weak Ignition Behind Incident Shock Waves and the Transition to Detonation". A more detailed and complete version of this work is presented in Appendix C entitled, "Ignition of Flamelets Behind Incident Shock Waves and the Transition to Detonation" and this has been accepted for publication in the journal, Combustion Science and Technology.

REFERENCES

1. Bach, G.G., Knystautas, R. and Lee, J.H.: Thirteenth Symposium (International) on Combustion, p. 1097, The Combustion Institute, 1971.
2. Lee. J.H., Knystautas, R. and Guirao, C.M.: Fifteenth Symposium (International) on Combustion, p. 53, The Combustion Institute, 1975.
3. Knystautas, R. and Lee, J.H.: Combust. Flame 27, 221 (1976).
4. Dabora, E.K.: Effect of Additives on the Lean Detonation Limit of Kerosene Sprays. UCONN0507-129-F, The University of Connecticut, 1980.
5. Abouseif, G.E. and Toong, T.Y.: Combust, Flame 45, 39 (1982).
6. Lee, E.L. and Tarver, C.M.: Phys. Fluids 23, 2362 (1980).
7. Meyer, J.W., and Oppenheim, A.K., Thirteenth Symposium (International) on Combustion, The Combustion Institute, Pittsburgh, 1971, pp. 1153-1164.
8. Strehlow, R.A., Crooker, A.J., and Cusy, R.E., Combust. Flame 11, 339 (1967).
9. Bazhenova, T.V., and Soloukhin, R.I., Seventh Symposium (International) on Combustion, The Combustion Institute, Pittsburgh, 1959, pp. 866-875.
10. Edwards, D.H., Thomas, G.O., and Williams, T.L., Combust. Flame 43, 187 (1981).

11. Oran, E.S., Young, T.R., Boris, J.P., and Cohen, A. Weak and Strong Ignition-I. Naval Research Laboratory Memorandum Report 4664, Washington, DC 1981 (also to appear in Combust. Flame).

12. Oran, E.S., Young, T.R., and Boris, J.P., Seventeenth Symposium (International) on Combustion, The Combustion Institute, Pittsburgh, 1979, pp. 43-54.

13. Oran, E.S., and Boris, J.P., Prog. Energy Combust. Sci. 7, 1. (1981).

14. Oran, E.S., Boris, J.P., Young, T., Flanigan, M., Burks, T., and Picone, M., Eighteenth Symposium (International) on Combustion, The Combustion Institute, Pittsburgh, 1981 pp. 1641-1649.

15. Oran, E.S. Young, T.R., Boris, J.P., and Picone, J.M., A Study of Detonation Structure: The Formation of Unreacted Gas Pockets. Presented at the Nineteenth Symposium (International) on Combustion, The Combustion Institute, Pittsburgh, 1982.

APPENDIX A

POWER-ENERGY RELATIONS FOR THE DIRECT INITIATION OF DETONATIONS IN OXY-ACETYLENE MIXTURES

POWER-ENERGY RELATIONS FOR THE DIRECT INITIATION OF DETONATIONS IN OXY-ACETYLENE MIXTURES

K. Kailasanath* and E.S. Oran
Laboratory for Computational Physics
Naval Research Laboratory
Washington, D.C. 20375

*Science Applications Inc., McLean, Virginia 22102

ABSTRACT

Recent experimental studies on the direct initiation of gaseous detonations have shown that initiation depends not only on the energy deposited but also on the rate at which it is deposited, namely the power. In this paper, we have used a theoretical model to determine the relation between the power and the energy required for the initiation of planar, cylindrical and spherical detonations in a detonable gas mixture. The results from the model show that the qualitative differences in the power-energy relations obtained from two different experimental arrangements are due to differences in the geometry. We also show that the minimum power requirement corresponds to a shock of minimum Mach number only in the case of planar detonations. Finally, the effect on the power-energy relation of the experimental uncertainties in the determination of the induction times has been studied for a stoichiometric oxy-acetylene mixture.

Introduction

The early studies of direct initiation of gaseous detonations[1,2,3] established the importance of the magnitude of the source energy. More recent experiments[4,5,6] have shown the importance not only of the energy but also of the rate at which the energy is deposited, namely the power. The experimental results of Lee et al.[5] indicate that there is a minimum detonation energy, E_m, below which a detonation would not occur no matter what the power is and that there is a minimum power, P_m, below which a detonation would not occur no matter what the total energy is. Later, they noted [6] that the requirement for a minimum value for the power of the source indicates that the source must be capable of generating a shock wave of certain minimum strength (Mach number). They also concluded that the minimum energy requirement implied that the shock wave must be maintained at or above this minimum strength for a certain minimum duration.

Recently these ideas have been used by Dabora[7,8] to obtain a relation between the power and energy required for the direct initiation of hydrogen-air detonations in a shock tube. However, this power-energy relation is very

different qualitatively from those of Knystautas and Lee[6]. More recently Abouseif and Toong[9] have proposed a simple theoretical model to determine the power-energy relation and predict their respective threshold values. The predictions based on their model were in qualitative agreement with the experiments of Knystautas and Lee[6].

In this paper we have modified and extended the basic model proposed by Abouseif and Toong[9] and have used it to determine the relation between the power and the energy required for the initiation of planar, cylindrical and spherical detonations in a detonable gas mixture. Specifically, we discuss its application to a stoichiometric oxy-acetylene mixture.

The Theoretical Model

The model considers the flow generated by the motion of a constant velocity shock wave in planar, cylindrical and spherical geometries. As this shock wave passes through a gas mixture, the gas temperature and pressure increases. Due to this increase in temperature and pressure, ignition could occur in the shock heated gas mixture after the elapse of a certain time and this may lead to a detonation.

A constant velocity shockwave can be formed in each of the three geometries by the motion of a constant velocity piston[10,11]. Furthermore, it has been shown[12] that a pressure and velocity field identical to that ahead of a constant velocity piston can be generated by appropriate heat addition. For example, a flow field bounded by a constant velocity planar piston and a constant velocity planar shock wave can be generated by a planar energy source with a constant rate of energy deposition. An example of such an energy source is the high pressure driver in a constant area shock tube.

In general, the source power P to generate a constant velocity piston in planar, cylindrical and spherical geometries can be written as[9,11]

$$P(t) = \frac{\gamma}{(\gamma-1)} C_\alpha p_p u_p^\alpha t^{\alpha-1} \quad , \tag{1}$$

where $C_\alpha = 1, 2\pi, 4\pi$ for $\alpha = 1,2,3$ corresponding to the planar, cylindrical and spherical geometries respectively; p_p and u_p are the pressure and velocity at the piston surface and t is the duration of energy deposition. The energy deposited is given by the time integral of the power, that is

$$E(t) = \frac{\gamma}{(\gamma-1)} \frac{C_\alpha}{\alpha} p_p u_p^\alpha t^\alpha \quad . \tag{2}$$

In the planar case, the pressure and fluid velocity at the piston surface are the same as those just behind the shock. However, in the cylindrical and spherical cases, the flow field between the shock and the piston surface is nonuniform and can be obtained by solving the governing partial differential equations. However, the solution procedure is considerably simplified if we seek a similarity solution. Then the system of partial differential equations can be reduced to a system of coupled ordinary differential equations:

$$\frac{(u-L)}{\rho} \frac{d\rho}{dL} + \frac{du}{dL} + (\alpha-1) \frac{u}{L} = 0 \tag{3}$$

$$(u-L) \frac{du}{dL} = -\frac{1}{\rho} \frac{dp}{dL} \tag{4}$$

$$\frac{dp}{dL} = \frac{\gamma p}{\rho} \frac{d\rho}{dL} \quad . \tag{5}$$

In the above system of equations, the density ρ, the velocity u and the pressure p are all functions of the similarity variable L, which is equal to the radial location r divided by the time t. The pressure and the velocity at the piston surface which are required in Eqs. (1,2) can be obtained by solving Eqs. (3-5) in the following manner. For a shock of a given Mach number, we can calculate the flow condition just behind the shock using normal shock relations. We can then integrate Eqs. (3-5) from just behind the shock to the piston surface to obtain p_p and u_p which are needed in Eqs. (1,2). The procedure is further simplified by appropriately combining Eqs. (3-5) into two equations and normalizing them. This is discussed in detail elsewhere[11].

In order to determine the power-energy relation using Eqs. (1,2) we also need to know the duration for which the energy must be deposited in order to initiate a detonation. This time must at least be equal to the time at which ignition first occurs in the flow field[9]. As noted by Urtiew and Oppenheim[13] ignition usually occurs first at the contact surface (i.e., at the piston surface here) since the temperature and pressure is highest at this location. So a first estimate of the time t in Eqs. (1,2) would be the induction delay time corresponding to the conditions at the piston surface.

Results and Discussion

We first used the model described above to determine the power-energy relation for the initiation of cylindrical detonations in a stoichiometric oxy-acetylene mixture. The initial temperature and pressure of the mixture were taken to be 300 K and 100 torr (0.1316 atm) to correspond to the initial conditions in the experiments of Knystautas and Lee[6]. As a first

approximation the time duration necessary for successful initiation was assumed to be equal to the chemical induction time of the mixture corresponding to the conditions at the piston surface. The induction time data used were those obtained by Edwards et al.[14] for an acetylene-oxygen-nitrogen (2:5:4) mixture and are given by:

$$\text{Log}\,(\tau[O_2]) = -9{\cdot}41 \pm 0.2 + \frac{71{\cdot}35 \pm 3{\cdot}34}{19{\cdot}14\ T} \qquad (6)$$

where τ is the induction time in seconds, $[O_2]$ is the concentration in mol/liter, and T is the temperature in thousands of degrees K. Three different power-energy relations obtained from the theoretical model are shown in Figure 1. Curve A was obtained by using the smallest value of the induction time given by Eq. (6), that is, by choosing the negative signs. Curve B was obtained by using the mean values and curve C by using the largest value of the induction time (by choosing the positive signs). The arrows on curve C indicate the direction of increasing Mach number. First, we note that each curve has a minimum power and a minimum energy. We also observe that as the Mach number decreases below the Mach number corresponding to the minimum power, both the average source power and the source energy increase. However, when the Mach number increases above the Mach number corresponding to the minimum power, the energy first decreases to the minimum energy and then increases again. All three curves exhibit these same qualitative trends.

The shape of these curves can be explained in the following manner. As the Mach number of the shock wave decreases, the pressure and the temperature behind it decrease. This decrease also results in a decrease of the pressure and velocity at the piston surface. This would tend to decrease both the

power and the energy since, as seen in Eqs. (1,2),

$$P \sim p_p u_p^2 t \qquad (7) \text{ and}$$

$$E \sim p_p u_p^2 t^2 \quad . \qquad (8)$$

This tendency is, however, opposed by the tendency of the induction time to increase with decreases in the pressure and the temperature. For low Mach numbers, (i.e., low temperatures behind the shock) a small decrease in the Mach number of the shock wave leads to a large increase in the induction time. The shape of the curves in Figure 1 implies that this increase in induction time is more than sufficient to compensate for the decrease in the pressure and the velocity for Mach numbers below that corresponding to the minimum power. Therefore both the power and the energy increase with decreasing Mach number. Since the energy is proportional to the product of the power and the induction time, (Eqs. (7,8)) the energy increases faster with induction time than the power does. As the Mach number increases above that corresponding to the minimum power, the increase in the pressure and velocity is larger than the decrease in the induction time. Therefore the power increases. However, for a certin range of Mach numbers, the increase in the pressure and velocity is not sufficient to compensate for the decrease in the square of the induction time. Therefore the energy decreases until it attains a minimum value, even though the power increases. Finally, for Mach numbers above that corresponding to the minimum energy, the increase in the pressure and velocity are easily able to overcome the decrease in the induction time with increasing Mach number and both the power and the energy increase. This occurs because the rate of decrease of the induction time

with temperature is small for high temperatures (i.e., high Mach numbers) according to Eq. (6).

The power-energy curve obtained using data from the spark ignition experiments[6] of Knystautas and Lee has also been included in Figure 1 as curve D. This curve exhibits the same qualitative trends as those of the theoretical curves discussed above. However, we observe that the values of the minimum power and the minimum energy from the four curves are very different from each other. The differences in the values of these parameters from the three "theoretical" curves (A,B, and C) indicate that the experimental uncertainties in the values of the induction times used have a significant effect on the value of the minimum power and the minimum energy. The minimum power varies from about 0.3 MW/cm to about 1 MW/cm and the minimum energy varies from about 0.012 J/cm to about 0.1 J/cm. The experimentally determined minimum power (from curve D) is about 0.13 MW/cm, which is lower than the calculated values, and the minimum energy is about 0.1 J/cm, which is at the top of the range of calculated values.

The quantitative differences between the exprimental and theoretical values could be due to a variety of factors. For example, there may be differences in the shape of the detonation wave in the experiments and the calculations. There are also uncertainties in the induction time data. We have used the induction time given by Eq. (6) for a range of temperatures far greater than that over which it was determined. As seen from Figure 1 and the discussion above, uncertainties in the induction time have a significant effect on the power-energy relations. Furthermore some of the approximations made in the theoretical model, such as the assumption that the similarity approximation is valid or that the appropriate time to be used in Eq. (1,2)

is the induction time, are also debatable. These factors and other limitations of the model have been studied and discussed in more detail by Kailasanath and Oran[11].

The derived power-energy relation for the initiation of planar detonations in the same oxy-acetylene mixture is shown in Figure 2. In this figure, we also show the shock tube data of Dabora[7] on the direct initiation of detonations in a stoichiometric hydrogen-air mixture. Both curves exhibit the same qualitative behavior. Unlike the cylindrical case, each value of the power corresponds to an unique value of energy. The direction of increasing shock strength (as determined by the Mach number) is also shown in Figure 2. In the planar case, we see that as the Mach number decreases the power always decreases. As noted earlier, in the cylindrical case, as the Mach number decreases, the power decreases only up to the minimum power. Then the power increases with a decrease in the Mach number of the shock wave. Therefore, the qualitative difference in the experimental data of Knystautas and Lee (shown in Figure 1) and Dabora (shown in Figure 2) are due to the difference in the geometry of the two detonations.

In Figure 2, we also observe that as the Mach number decreases, we need more and more energy to initiate a detonation. The trend of the curves indicates that there is a minimum Mach number below which a detonation will not occur (i.e., would require an infinite amount of energy). The value of the power corresponding to this minimum Mach number is the minimum power. This agrees with the observation made by Lee et al.[6] that the requirement for a minimum value of the source power indicates that the source must be capable of generating a shock wave of a certain minimum Mach number. However, we observe from Figure 1 that for the case of cylindrical detonations, the

minimum power does not correspond to the shock wave of minimum Mach number. In the cylindrical case, it is possible to initiate a detonation with a shock wave of lower Mach number than that corresponding to the minimum power. Such a shock will have to be maintained for a longer time than the shock corresponding to the minimum power and hence will require a larger amount of energy.

The power-energy curve for the initiation of spherical detonations is similar to the curve for the cylindrical case. However, for the case of spherical detonations, the power,

$$P \sim p_p u_p^3 t^2 \tag{9}$$

but we still have the energy,

$$E \sim P t \tag{10}$$

Since the power and energy are proportional to higher powers of the time, t, uncertainties in t will have a greater effect on the value of the minimum power and the minimum energy. Further work is being carried out currently to study the initiation of spherical detonations in hydrogen-air mixtures and to compare it with experimental data.

Conclusions

The results discussed above show that though the simple theoretical model has significant limitations, it can still be used to explain the qualitative differences in the power-energy relations obtained from different experimental arrangements. The results from the model also show that the minimum power and the minimum detonation energy are very sensitive to uncertainties in the ignition delay time used. Another interesting conclusion

from the model is that the minimum power requirement corresponds to a shock of minimum Mach number only in the case of planar detonations. Currently, further applications of the model and extensions to the study of condensed phase detonations are being considered.

Acknowledgements

The authors greatfully acknowledge suggestions, useful conversations and help from Jay P. Boris and T.R. Young. The authors also acknowledge the editorial assistance of Ms. F. Rosenberg. This work has been supported by the Office of Naval Research through the Naval Research Laboratory.

References

1. Zeldovich, Y.B., Kogarko, S.M. and Simonov, N.N.: Soviet Phys.-JETP 1, 1689 (1956).

2. Litchfield, E.L., Hay, M.H. and Forshey, D.R.: Ninth Symposium (International) on Combustion, p. 282, Academic Press, 1963.

3. Freiwald, H. and Koch, H.W.: Ninth Symposium (International) on Combustion, p. 275, Academic Press, 1963.

4. Bach, G.G., Knystautas, R. and Lee, J.H.: Thirteenth Symposium (International) on Combustion, p. 1097, The Combustion Institute, 1971.

5. Lee, J.H., Knystautas, R. and Guirao, C.M.: Fifteenth Symposium (International) on Combustion, p. 53, The Combustion Institute, 1975.

6. Knystautas, R. and Lee, J.H.: Combust. Flame 27, 221 (1976).

7. Dabora, E.K.: Effect of Additives on the Lean Detonation Limit of Kerosene Sprays. UCONN0507-129-F, The University of Connecticut, 1980.

8. Dabora, E.K.: The Relation between Energy and Power for Direct Initiation of Hydrogen-Air Detonations. Presented at the Second International Workshop on the Impact of Hydrogen on Water Reactor Safety, Albuquerque, New Mexico, Oct. 1982.

9. Abouseif, G.E. and Toong, T.Y.: Combust. Flame 45, 39 (1982).

10. Taylor, G.I.: Proc. Roy. Soc. A. 186, 273 (1946).

11. Kailasanath, K. and Oran, E.S.: The Relation between Power and Energy for the Direct Initiation of Gaseous Detonations. NRL Memorandum Report (in preparation, 1983).

12. Chu, B.T.: NACA TN 3411, 1955.

13. Urtiew, P.A. and Oppenheim, A.K.: Eleventh Symposium (International) on Combustion, p. 665, The Combustion Institute, 1967.

14. Edwards, D.H., Thomas, G.O. and Williams, T.L.: Combust. Flame 43, 187 (1981).

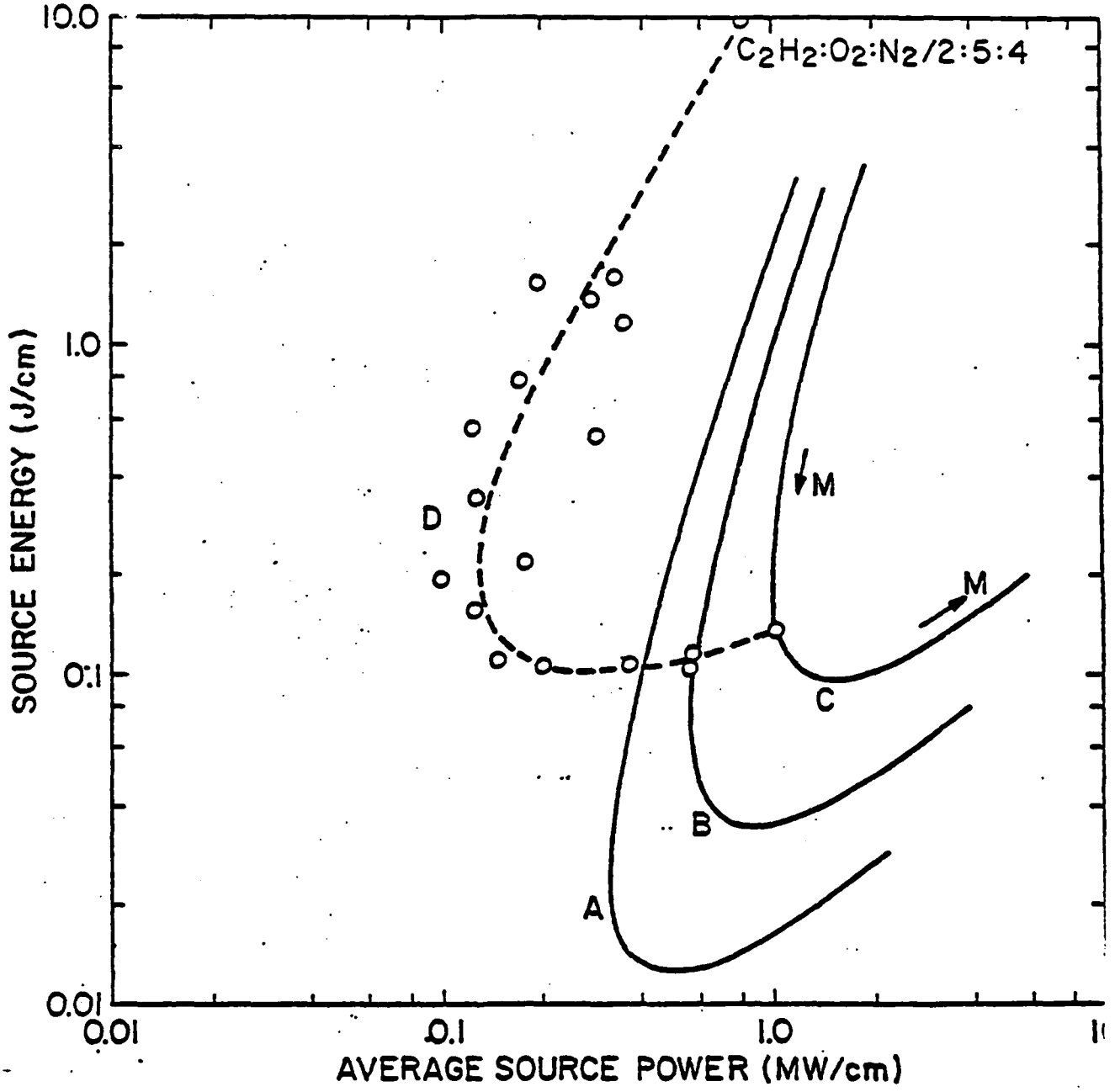

Figure 1. Power-energy relations for the initiation of cylindrical detonations in an acetylene-oxygen-nitrogen mixture (2:5:4) at 1 atm and 300 K. Curve D is obtained from spark ignition experiments (6). Curves A, B, and C are explained in the text. The arrows on Curve C indicate the direction of increasing Mach number.

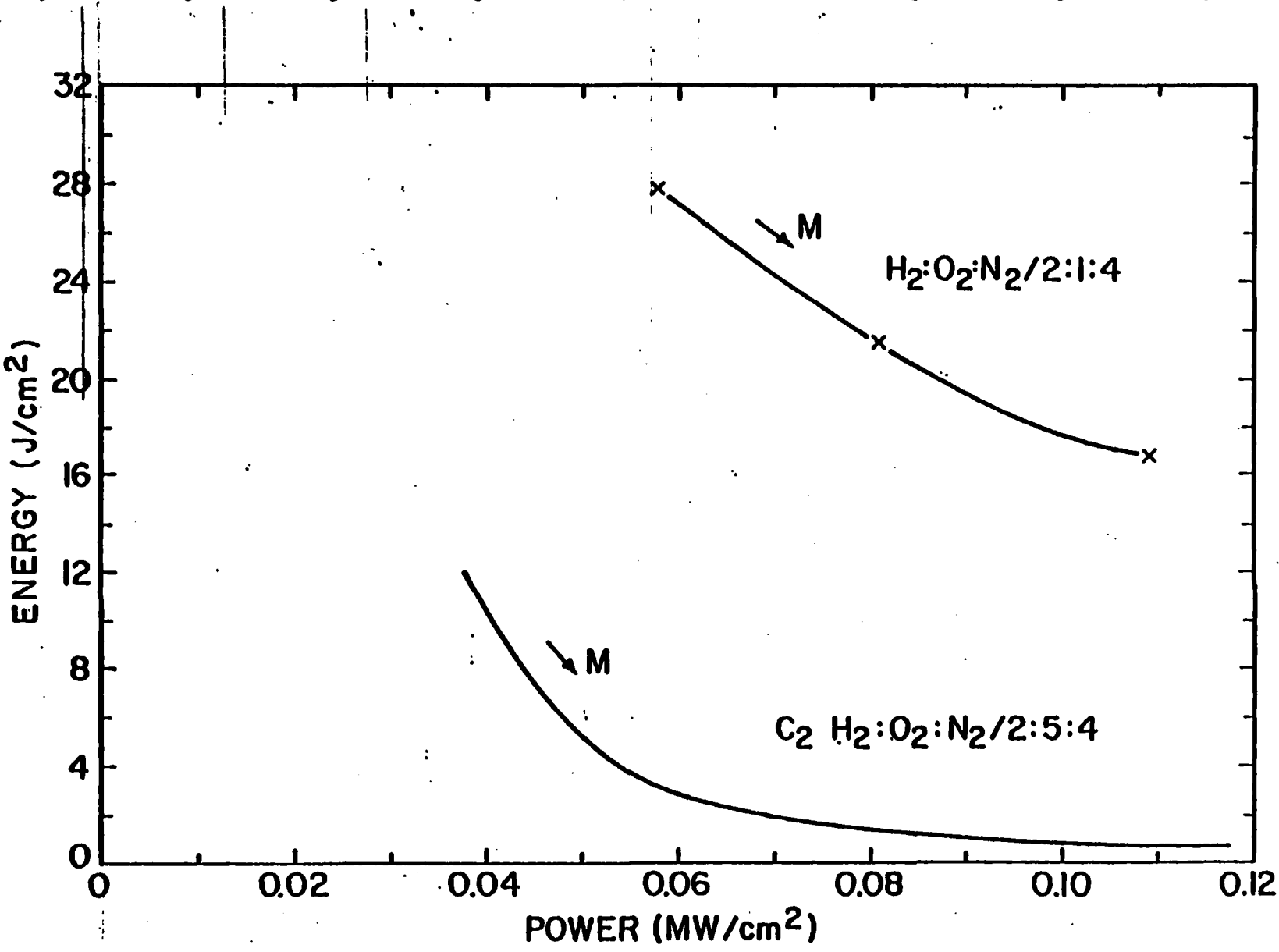

Figure 2. Power-energy relations for the initiation of planar detonations. The x's are data obtained from shock tube experiments (7).

APPENDIX B

NUMERICAL SIMULATIONS OF WEAK IGNITION BEHIND INCIDENT SHOCK WAVES AND THE TRANSITION TO DETONATION

Numerical Simulations of Weak Ignition Behind Incident Shock Waves and the Transition to Detonation

K. Kailasanath* and E.S. Oran
Laboratory for Computational Physics
Naval Research Laboratory
Washington, DC 20375

Introduction

Shock induced ignition in gaseous hydrogen-air mixtures may occur in one of two distinct modes, depending on the thermodynamic state in the shocked material. At lower temperatures the ignition is weak, or mild, with the gradual development of the gas dynamic explosion; at higher temperatures it is strong, or sharp, with a practically instantaneous appearance of a secondary shock induced by the explosive reaction. Furthermore at low temperatures the formation of distinct flame kernels appears to be an essential precursor of ignition. Meyer and Oppenheim [1] point out that the intrinsically turbulent flow field behind a reflected shock in a shock tube results in a nonuniform temperature distribution which creates distinct reaction centers and leads to weak ignition. Although the nonuniformity of temperature caused by turbulence is one mechanism which gives rise to reaction centers, the nonsteadiness in the velocity of the causal shock can also produce them. This latter effect has been convincingly demonstrated by Strehlow et al. [2] in their studies of shock propagation in a slowly converging channel. It has also been shown that when an incident shock in a uniform shock tube begins to accelerate, hot spots occur before the transition to detonation [3,4].

We present results from time-dependent numerical simulations used to elucidate some of the details of weak ignition behind incident shock waves and the subsequent transition to detonation. These simulations were performed using a one-dimensional model [5,6] which combines a description of the fluid dynamics and detailed chemical kinetics. With such detailed one-dimensional numerical simulations one hopes to isolate and study some of the various phenomena occuring in actual multi-dimensional systems.

The Numerical Model

The one-dimensional reactive shock model [5,6] used to perform the calculations described below solves the time-dependent conservation equations [7] for mass, momentum and energy coupled to the equations describing the chemical kinetics. The model uses an explicit, Eulerian finite difference formulation with a sliding rezone capability to provide resolution around moving gradients. The solutions of the equations describing the fluid dynamics and the chemistry of the problem are coupled using time-step splitting techniques [6].

The convective transport terms in the conservation equations are solved using one variant of the Flux-Corrected Transport (FCT) method [8]. This is a conservative, monotonic algorithm with fourth-order phase accuracy and does not require artificial viscosity to stabilize shocks. The ordinary differential equations describing the chemical kinetics are solved using

*Currently with Science Applications, Inc. McLean, VA.

VSAIM, a vectorized version of the selected asymptotic integration method employed in CHEMEQ [9]. The chemical kinetics rate scheme used consists of about fifty rates relating the species H_2, O_2, H, O, OH, HO_2, H_2O and H_2O_2 and has been extensively tested against experimental data [10,11].

Results and Discussion

In the shock tube simulations, the pressure across the diaphragm and the driven gas mixture are chosen so that the thermodynamic state behind the incident shock is in the weak ignition regime [12]. Figure 1 is a position-time diagram of the events occurring in the shock tube simulation. The trajectory of the shock front is labelled S and that of the contact surface is labelled CS. Five different regimes have also been identified on the diagram. They are (a) pre-ignition regime, (b) quasi-steady shock-reaction complex, (c) formation of reactive centers, (d) hot spot formation leading to an overdriven detonation and (e) detonation relaxation. Similar regions have been identified by Edwards et al. [4] in their shock tube experiments. These regions are examined in detail below.

Initially, the shock travels at a nearly constant velocity (1.4×10^5 cm/s) into the hydrogen-air mixture, raising its temperature and pressure to a near-constant value. Gradually reactions begin to occur in the shock heated gas. Small pressure disturbances due to energy release travel forward at a velocity of 1.8×10^5 cm/s (in the laboratory frame of reference), which is the sum of the sonic and particle velocities behind the shock. When they reach the shock they accelerate the shock slightly. Once the shock is accelerated, the temperature of the gases now passing through the shock is higher than the raised temperature created by the original shock. In the weak-ignition regime, such an increase in temperature can result in a significant reduction in the induction time [12, 13]. The numerical simulations show how this leads to the formation of reactive centers (RC) in the newly shocked material. At these reactive centers, reaction progresses at a much move rapid rate than in the previously shocked material. The development of a hot spot due to energy release at one of the reactive centers can be seen in the simulations. The presence of such hot spots has been observed earlier in shock tube experiments [2,4].

Energy release at a hot spot causes a pair of flamelets or reaction waves (RW), one propagating ahead into the shock heated gas mixture and the other propagating back towards the contact surface. These flamelets initially propagate at a subsonic speed with respect to the fluid. Such flamelets have been observed by Bazhenova and Soloukhin [3] in their incident shock tube experiments. Energy release behind these flamelets causes pressure waves which accelerate the flamelets into detonation type waves. The reaction wave moving backward against the fluid accelerates slowly and travels at nearly the sonic speed till it reaches the contact surface. However the forward moving reaction wave transitions into a strong detonation wave even before it reaches the incident shock wave. This agrees with the observation made by Bazhenova and Soloukhin [3] that the merging of the flame front with the incident shock wave is not a necessary condition for the detonation wave formation.

The numerical simulations presented in this paper show that the one-dimensional reactive flow model with detailed chemical kinetics can be used to elucidate some of the details of weak ignition behind incident shocks and the subsequent transition to detonation. The predictions of the model are in qualitative agreement with experimental observations. However, the model does not include multi-dimensional phenomena such as turbulence and boundary layer growth which play an important part in any quantitative study of the transition to detonation. Currently a two-dimensional reactive shock model exists but it uses a parameterized model for energy release [14,15]. The model is now being extended to include a detailed chemical kinetic scheme. Calculations such as shown here performed with this model would show the effects of transverse waves and boundary layers on the transition to detonation.

This work has been supported by the Office of Naval Research through the Naval Research Laboratory.

References

1. Meyer, J.W., and Oppenheim, A.K., Thirteenth Symposium (International) on Combustion, The Combustion Institute, Pittsburgh, 1971, pp. 1153-1164.
2. Strehlow, R.A., Crooker, A.J., and Cusy, R.E., Combust. Flame., 11, 339 (1967).
3. Bazhenova, T.V., and Soloukhin, R.I., Seventh Symposium (International) on Combustion, The Combustion Institute, Pittsburgh, 1959, pp. 866-875.
4. Edwards, D.H., Thomas, G.O., and Williams, T.L., Combust. Flame. 43, 187 (1981).
5. Oran, E.S., Young T.R., and Boris, J.P., Seventeenth Symposium (International) on Combustion, The Combustion Insititute, Pittsburgh, 1979, pp. 43-54.
6. Oran, E.S., and Boris, J.P., Prog. Energy Combust. Sci. 7, 1. (1981).
7. Williams, F.A. Combustion Theory, Addison-Wesley, Reading, 1965 p. 2.
8. Boris, J.P., and Book, D.L., Solution of Continuity Equations by the Method of Flux-Corrected Transport. In Methods of Computational Physics, Academic Press, New York, 1976, Vol. 16, Chap. 11, pp. 85-129.
9. Young, T.R., and Boris, J.P., J. Phys. Chem. 81, 2424 (1977).
10. Oran, E.S. Young, T.R., Boris, J.P., and Cohen, A. Weak and Strong Ignition-I. Naval Research Laboratory Memorandum Report 4664, Washington, DC 1981 (also to appear in Combust. Flame).
11. Burks, T.L., and Oran, E.S., A Computational Study of the Chemical Kinetics of Hydrogen Combustion. Naval Research Laboratory Memorandum Report 4446, Washington, DC, 1980.
12. Oran, E.S., and Boris, J.P., Weak and Strong Ignition-II. Naval Research Laboratory Memorandum Report 4671, Washington, DC, 1981 (also to appear in Combust. Flame).
13. Meyer, J.W., and Oppenheim, A.K. Combust. Flame. 17, 65 (1971).
14. Oran, E.S., Boris, J.P., Young, T., Flanigan, M. Burks, T., and Picone, M., Eighteenth Symposium (International) on Combustion, The Combustion Institute, Pittsburgh, 1981, pp. 1641-1649.
15. Oran, E.S., Young, T.R., Boris, J.P., and Picone, J.M., A Study of Detonation Structure: The Formation of Unreacted Gas Pockets. Presented at the Nineteenth Symposium (International) on Combustion, The Combustion Institute, Pittsburgh. 1982.

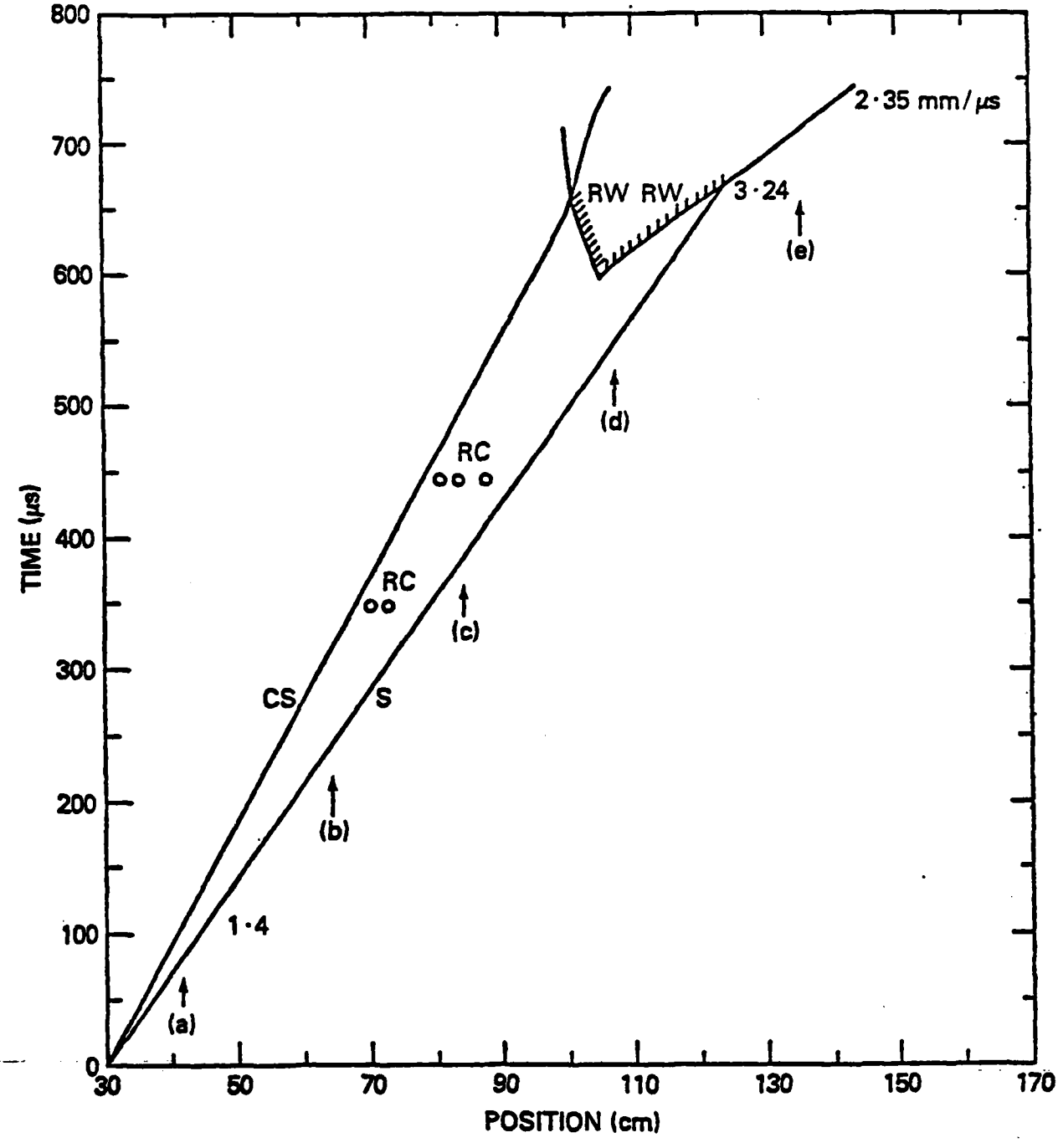

Figure 1. A position-time diagram of the main events occurring in the shock tube simulation. The symbols are explained in the text.

APPENDIX C

IGNITION OF FLAMELETS BEHIND INCIDENT SHOCK WAVES AND THE TRANSITION TO DETONATION

IGNITION OF FLAMELETS BEHIND INCIDENT SHOCK WAVES AND THE TRANSITION TO DETONATION

K. Kailasanath* and E.S. Oran

Laboratory for Computational Physics

Naval Research Laboratory

Washington, DC 20375

*Currently with Science Applications, Inc., McLean, VA

ABSTRACT

Time-dependent numerical simulations are used to elucidate some of the details of weak ignition behind incident shocks and the subsequent transition to detonation. It is shown that a small amount of energy released in the shocked region can be the origin of pressure waves which accelerate the shock front. The simulations presented here show how this leads to the formation of reactive centers. The formation of a hot spot due to energy release at one of the reactive centers and the subsequent development of a pair of flamelets from the hot spot are studied using the numerical simulations. The results of the simulations are also compared to experimental observations.

I. INTRODUCTION

Shock-induced ignition in gaseous hydrogen-air mixtures may occur in one of two distinct modes, depending on the thermodynamic state in the shocked material. At lower temperatures the ignition is weak, or mild, with the gradual development of the gas dynamic explosion. At higher temperatures it is strong, or sharp, with an abrupt appearance of a secondary shock induced by the explosive reaction. Furthermore at low temperatures the formation of distinct flame kernels appears to be an essential precursor of ignition. Meyer and Oppenheim (1971a) point out that the intrinsically turbulent flow field behind a reflected shock in a shock tube results in a nonuniform temperature distribution which creates distinct reaction centers and leads to weak ignition. Although the nonuniformity of temperature caused by turbulence is one mechanism which gives rise to reaction centers, the nonsteadiness in the velocity of the causal shock can also produce them. This latter effect has been convincingly demonstrated by Strehlow et al. (1967) in their studies of shock propagation in a slowly converging channel. It has also been shown that when an incident shock in a uniform shock tube begins to accelerate, hot spots occur before the transition to detonation (Bazhenova and Soloukhin, 1959; Edwards et al., 1981).

In this paper the reactive flow behind an incident shock wave in a hydrogen-air mixture is simulated using a one-dimensional, time-dependent numerical model which combines a description of the fluid dynamics and detailed chemical kinetics. In the simulations, the pressure ratio across the diaphragm and the driven gas mixture are chosen so that the thermodynamic

state behind the incident shock is in the weak ignition regime (Oran and Boris, 1981b). It is shown that a small amount of energy released in the shocked gas (which might occur due to density, temperature or stoichiometric fluctuations) can be the origin of pressure waves which accelerate the shock front. Once the shock is accelerated, the temperature of the gases now passing through the shock is higher than the raised temperature created by the original shock. In the weak ignition regime, such an increased temperature can result in a significant reduction in the induction time (Meyer and Oppenheim. 1971b; Oran and Boris, 1981b). The simulations presented here show how this leads to the formation of reactive centers in the newly shocked material where reaction progresses at a more rapid rate than in the previously shocked material. The formation of a hot spot due to energy release at one of the reactive centers and the subsequent development of a pair of flamelets or reaction waves from the hot spot are studied using the numerical simulations. The results of the simulations have also been compared to experimental observations (Bazhenova and Soloukhin, 1959; Urtiew and Oppenheim, 1966, 1967; Strehlow et al., 1967; Edwards et al., 1981).

II. THE NUMERICAL MODEL

The one-dimensional reactive shock model (Oran et al., 1979; Oran and Boris, 1981a) used to perform the calculations described below solves the time-dependent conservation equations (Williams, 1965; Oran and Boris, 1981a) for mass, momentum and energy coupled to the equations describing the chemical kinetics. The model uses an explicit, Eulerian finite difference formulation with a sliding rezone capability to provide resolution around moving gradients. The solutions of the equations describing the fluid

dynamics and the chemistry of the problem are coupled using time-step splitting techniques (Oran and Boris, 1981a).

The convective transport terms in the conservation equations are solved using one variant of the Flux-Corrected Transport (FCT) method (Boris and Book, 1976; Boris, 1976). This is a conservative, monotonic algorithm with fourth-order phase accuracy and does not require artificial viscosity to stabilize shocks. The Flux Correction procedure itself ensures that the shocks are one or two zones wide and have maximal resolution. The ordinary differential equations describing the chemical kinetics are solved using VSAIM, a vectorized version of the selected asymptotic integration method employed in CHEMEQ (Young and Boris, 1977; Young, 1980). This algorithm identifies the stiff equations for treatment with a stiffly stable method. The remaining equations are solved with a standard classical method. The algorithm has been specially optimized for use in conjunction with fluid dynamic models.

The chemical kinetics rate scheme used is given in Table I. It consists of about fifty rates relating the species H_2, O_2, H, O, OH, HO_2, H_2O and H_2O_2 and has been extensively tested against experimental data (Oran et al., 1981, Burks and Oran, 1980). Burks and Oran (1980) showed that the results computed with the scheme compared very well with experimentally observed induction times, second explosion limits and the temporal behavior of reactive species. Oran et al. (1981) have shown that the scheme gives good results when coupled with a fluid dynamic model in the simulation of the conditions behind a reflected shock. Heats of formation and enthalpies have been taken from the JANAF tables (1971).

For the calculations performed in this paper, the timescales under consideration are short and therefore the diffusive transport processes, thermal conduction and molecular diffusion, have negligible effect. The effects of these processes have not been considered although they are part of the general numerical model. Although the geometry may be either cartesian, cylindrical, spherical or some generalized co-ordinate, the simulations presented below are in cartesian geometry.

The detailed simulations discussed in this paper require that we model relatively long systems (on the order of meters) while we simultaneously maintain high accuracy around steep gradients such as the shock front and the contact surface. The rather sophisticated adaptive gridding method developed for this purpose is shown schematically in Figure 1. There are two finely gridded regions: One surrounding the shock wave and the other surrounding the contact surface. The fine-zoned region around the contact surface moves with the contact surface at the fluid velocity, and so this part of the calculations is essentially Lagrangian. The region around the shock front moves with the front. Each of these finely gridded regions may have a different minimum computational cell size. The computational cells in the regions ahead of the shock wave and behind the contact surface change exponentially in size from the smallest near the shock wave or the contact surface to the largest at the walls. Care is taken that the transition in the cell sizes is smooth. For the results presented in this paper a total of 200 computational cells are used to describe the shock tube and the cell sizes varied from 0.1 cm around the shock to over 50 cm near the shock tube end-walls.

III. WEAK IGNITION BEHIND AN INCIDENT SHOCK

The numerical model described in the preceding section was used to study weak ignition behind planar incident shock waves. The system parameters, the initial conditions and the temperature and pressure behind the incident shock have all been summarized in Table II. The chemical induction time, for the conditions described by the incident shock, is about 2000 μs. However, since the thermodynamic state behind the shock is in the weak ignition regime, ignition may occur much earlier than 2000 μs due to temperature, pressure, or density fluctuations.

Figure 2 is a position-time diagram of the events occurring in the shock tube simulation. The trajectory of the shock front is labelled S and that of the contact surface is labelled CS. Except for small variations (which are examined in detail below) the shock travels at a nearly constant velocity, 1.4×10^5 cm/s, until the reaction wave formed between the contact surface and the shock front reaches it. At this time the velocity rises quickly to 3.24×10^5 cm/s. It then gradually decreases towards the Chapman-Jouguet detonation velocity. Five different regimes have also been identified on the diagram. They are (a) pre-ignition regime, (b) quasi-steady shock-reaction complex, (c) formation of reactive centers, (d) hot spot formation leading to an overdriven detonation and (e) detonation relaxation. Similar regions have been identified by Edwards et al. (1981) in their shock tube experiments. These regions are examined in detail below.

As the shock travels at a nearly constant velocity into the hydrogen-air mixture, the temperature and pressure of the mixture are raised to a near-constant value. Reactions in the shock heated gas first occur near the

contact surface since the temperature has been high for the longest time here, as has been observed by Urtiew and Oppenheim (1967). In Figure 3, the spatial variation of the temperature and the OH mole fraction between the shock and the contact surface are shown at 135 μs after the bursting of the diaphragm. The OH mole fraction attains a maximum value near the contact surface and decreases across the system towards the shock front. This is because the gas mixture at different locations has been at the higher temperature for different durations.

Formation of Reactive Centers and Hot Spots

Small pressure disturbances occur due to the energy released in the reactions near the contact surface. These pressure disturbances travel forward at a velocity (in the laboratory frame of reference) of 1.8×10^5 cm/s, which is the sum of the sonic and particle velocities behind the shock. When they reach the shock they accelerate the shock slightly resulting in a temperature increase behind the shock. This can be observed in Figure 4 where the spatial distribution of the temperature between the shock and the contact surface is shown at four different times. The nonuniform temperature distributions can be explained by the following sequence of events: pressure disturbances originating at different times near the contact surface reach the incident shock at different times and each successive pressure disturbance meets a shock of slightly different strength because the shock has already been accelerated slightly due to previous pressure disturbances. We know that in the weak ignition regime, the induction time is very sensitive to perturbations in temperature and pressure (Oran and Boris, 1981b). This sensitivity, in fact, is what produces the two peaks in OH mole

fraction distribution (Figure 5A) at 348 μs after the bursting of the diaphragm. The first peak is due to the development of reactions near the contact surface and occurs in the same reactive center (see Figure 2) which was observed earlier. Now a second reactive center has formed closer to the shock front due to the higher temperature created by the acceleration of the shock. Again we observe that the reactive center occurs in that part of the shock heated gas which was at the elevated temperature for the longest period of time. Ahead of the second reactive center the rapid decrease in the radical mole fraction is halted by a further increase in the temperature behind the shock and a third reactive center is forming. By 445 μs (Figure 5B), a third reactive center has developed and the radical mole fraction is rising most rapidly at this center. The temperature around this reactive center is significantly (about 40° K) greater than that behind the initial incident shock wave. In the weak ignition regime, such changes in temperature result in a substantial reduction in the induction time. Therefore reaction progresses at this reactive center at a much more rapid rate than at any other location in the system. This results in a "hot spot" in the system. The development of this hot spot can be seen in Figure 6 where the temperature-distribution between the contact surface and the shock front has been shown for four different times. The temperature increases by more than 200° in 30 μs.

Transition to Detonation

The events occurring after the hot spot formation can be seen in Figure 7 where a segment of the position-time diagram (Figure 2) is presented in greater detail. The hot spot (marked "A" in the figure) travels with the

fluid and continuously releases energy into it. This results in "flamelets" or "reaction waves" ("B") which travel with respect to the fluid. One reaction wave moves forward with the fluid while another moves against the fluid towards the driver section. These reaction waves initially move subsonically with respect to the fluid but are soon accelerated into steep detonation type waves which move supersonically with respect to the fluid. When the forward moving reaction wave reaches the shock front, the shock velocity abruptly increases to a high value. The shock-reaction complex then moves as a strong overdriven detonation wave which decelerates towards the Chapman-Jouguet detonation velocity.

The temperature, pressure and velocity distributions across the system at a particular time after the hot spot has formed are shown in Figure 8a. By this time the energy release has resulted in a noticeable pressure rise. This occurs because the energy release is occurring at nearly constant volume conditions. The energy release at the hot spot causes a series of minute pressure pulses to propagate both forward and backward, each a little stronger than the previous one. A series of pressure pulses are produced since the energy release occurs over a period of time and is determined at each time from the detailed chemical kinetic interactions among the various species. These pressure pulses coalesce to form steepening pressure waves propagating into the shocked mixture as seen in Figure 8b. The time history of these reaction waves has been shown in a series of figures (Fig. 8b - Fig. 10b) which cover the time period between 609 μs and 688 μs.

Let us first look at the development of the reaction wave which moves forward into the shock-heated gas mixture. The velocity of the forward

moving wave, the fluid velocities on both sides of the wave and the speed of sound in the gas mixtures on both sides of the wave are given in Table III for a series of times. At 609 μs, the forward moving reaction wave is supersonic. The velocity of the fluid with respect to the wave decreases across the wave but is supersonic on either side. Furthermore the pressure rise across the wave is just over a factor of two, which is moderate. Thus the reaction wave behaves like a weak detonation wave at this time. Later, as seen in Figure 9a, the pressure rise across the wave has increased and the wave is also travelling faster. The velocity of the fluid with respect to the wave is still supersonic on both sides of the wave. The pressure rise across the wave continues to increase and at the time corresponding to Figure 9b, the fluid velocity behind the wave is nearly sonic. The weak detonation seems to be transitioning into a strong detonation. It does so later (Figure 9c) when the fluid velocity changes from supersonic to subsonic across the reaction wave. The pressure rise across the wave is also larger now. The observed acceleration of the forward moving wave into a strong detonation is due to the nonlinear interaction between chemical kinetics and fluid dynamics. When the forward moving wave moves into the previously shocked material there is a large pressure and temperature rise across it since it is a strong compressive wave. This increase in the pressure and the temperature reduces the induction time of the material which crossed the wave. Energy release in this newly re-compressed material accelerates the forward moving wave further, and this cycle is repeated until the forward moving wave reaches the incident shock wave (Figure 10a). By this time the pressure spike behind the reaction wave has risen to 6.6×10^6 dynes/cm^2. Because the

reaction wave is moving towards the incident shock at a speed greater than the local speed of sound in the shock-heated gas, there is no advance warning of the over-pressure region until the main spike physically arrives at the shock front. When the reaction wave does coalesce with the shock, there is a very rapid increase in the shock speed (Figure 7) and the shock-reaction wave complex moves as an overdriven strong detonation wave. Due to the high over-pressure that was associated with the reaction front, the detonation wave overshoots the Chapman-Jouguet value by a substantial amount. However, the overshoot cannot be sustained by the reaction and the overdriven detonation gradually relaxes towards a Chapman-Jouguet wave. By 688 μs (Figure 10b) the pressure spike behind the detonation wave has decreased to 4.8×10^6 dynes/cm^2 and the wave is moving faster than the C-J velocity by only 36%. In Figure 10b we also observe a small amplitude pressure wave moving into the detonation products. This pressure wave was formed when the reaction wave interacted with the shock front.

Let us now look at the reaction wave which moves backward towards the driver section. From Figure 7 and Table IV we see that this wave moves at nearly the sonic speed. The fluid velocity with respect to the wave is supersonic on either side of the wave. The pressure rise and the acceleration of the wave are slower since the wave is moving against the fluid. The pressure increase behind the wave is broader (Figure 9c) and smaller than that of the forward moving wave. It continues to propagate like a weak detonation wave until it interacts with the contact surface (Figure 10a). This interaction produces a pressure pulse which travels into the helium driver gas. In Figure 10b we see that this pressure pulse has produced a slight temperature increase in the helium.

IV. DISCUSSION AND CONCLUSIONS

In this paper the reactive flow behind an incident shock wave has been studied using a time-dependent numerical model which includes both detailed chemical kinetics and one-dimensional fluid dynamics. The numerical simulations show that the incident shock initially travels at a steady speed leaving behind it material in what has been called a "quasi-steady reaction complex". From their extensive experimental studies on detonation, Lee et al. (1976, 1977) have concluded that such regimes are universal predetonation phenomena. This regime has also been observed in the incident shock tube experiments of Edwards et al. (1981).

The calculations have also shown the acceleration of the shock due to pressure waves created by energy release in the shock heated gas mixture, a phenomenon also observed by Edwards et al. (1981). Shock acceleration raises the temperature of the gases passing through the shock and in the weak ignition regime, this results in a significant reduction of the induction time (Meyer and Oppenheim, 1971b; Oran and Boris, 1981b). This leads to the formation of reactive centers where reaction progresses at a more rapid rate than in the previously shocked material. The development of a hot spot due to energy release at one of the reactive centers has been shown in Figure 6. The presence of such hot spots has been observed earlier in shock tube experiments (Strehlow et al., 1967, Edwards et al., 1981).

Energy release at a hot spot causes a pair of flamelets or reaction waves, one propagating ahead into the shock heated gas mixture and the other propagating back towards the contact surface. These flamelets initially propagate at a subsonic speed with respect to the fluid. Such flamelets have

been observed by Bazhenova and Soloukhin (1959) in their incident shock tube experiments. Energy release behind these flamelets causes pressure waves which accelerate the flamelets into detonation type waves. The reaction wave moving backward against the fluid accelerates slowly and travels at nearly the sonic speed till it reaches the contact surface. However the forward moving reaction wave transitions into a strong detonation wave even before it reaches the incident shock wave. This agrees with the observation made by Bazhenova and Soloukhin (1959) that the merging of the flame front with the incident shock wave is not a necessary condition for the detonation wave formation. The simulations also show a large pressure overshoot when the forward moving wave coalesces with the incident shock wave. This has been observed earlier in the experiments of Urtiew and Oppenheim (1966).

The numerical simulations presented in this paper show that the one-dimensional reactive flow model with detailed chemical kinetics can be used to elucidate some of the details of weak ignition behind incident shocks and the subsequent transition to detonation. The predictions of the model are in qualitative agreement with experimental observations. However, the model does not include multi-dimensional phenomena such as turbulence and boundary layer growth which play an important part in any quantitative study of the transiton to detonation. Currently a two-dimensional reactive shock model exists but it uses a parameterized model for energy release (Oran et al., 1981b; Oran et al., 1982). The model is now being extended to include a detailed chemical kinetic scheme. Calculations with this new model would show the effects of transverse waves and boundary layers on the transition to detonation.

ACKNOWLEDGEMENTS

The authors greatfully acknowledge suggestions from and useful conversations with Jay Boris, Ted Young, and Antoni Oppenheim and editorial assistance from Mrs. Fran Rosenberg. This work has been supported by the Office of Naval Research through the Naval Research Laboratory.

REFERENCES

Bahn, G.S. (1968). Reaction Rate Compilation for H-O-N System, Gordon and Breach, New York.

Baulch, D.L., Drysdale, D.C., Horne, D.C., and Lloyd, A.C. (1972). Evaluated Kinetic data for High Temperature Reactions, Vol. 1, Butterworths, London.

Bazhenova, T.V., and Soloukhin, R.I. (1959). Gas Ignition Behind the Shock Wave. Seventh Symposium (International) on Combustion, The Combustion Institute, Pittsburgh, pp. 866-875.

Boris, J.P. (1976). Flux-Corrected Transport Modules for Solving Generalized Continuity Equations. Naval Research Laboratory Memorandum Report 3237, Washington, D.C.

Boris, J.P., and Book, D.L. (1976). Solution of Continuity Equations by the Method of Flux-Corrected Transport. In Methods of Computational Physics, Academic Press, New York, Vol. 16, Chap. 11, pp. 85-129.

Burks, T.L., and Oran, E.S. (1980). A Computational Study of the Chemical Kinetics of Hydrogen Combustion. Naval Research Laboratory Memorandum Report 4446, Washington, D.C.

Cohen, N., and Westberg, K.R. (1979). Data Sheets, The Aerospace Corporation, Los Angeles.

Edwards, D.H., Thomas, G.O., and Williams, T.L. (1981). Initiation of Detonation by Steady Planar Incident Shock waves, Combust. Flame. 43, 187.

Hampson, R.F., and Garvin, D. (1975). Chemical Kinetic and Photochemical Data for Modeling of Atmospheric Chemistry, NBS Technical Note 866, U.S. National Bureau of Standards, Washington, D.C.

Lee, J.H., and Ramamurthi, K. (1976). On the Concept of the Critical Size of a Detonation Kernal. Combust. Flame. 27, 331.

Lee, J.H. (1977). Initiation of Gaseous Detonation. Ann. Rev. Phys. Chem. 28, 75.

Lloyd, A.C. (1974). Evaluated and Estimated Kinetic Data for Gas Phase Reactions of the Hydroperoxyl Radical. Int. J. Chem. Kinetics. 6, 169.

Meyer, J.W., and Oppenheim, A.K. (1971a). On the Shock-Induced Ignition of Explosive Gases. Thirteenth Symposium (International) on Combustion, The Combustion Institute, Pittsburgh, pp. 1153-1164.

Meyer, J.W., and Oppenheim, A.K. (1971b). Coherence Theory of the Strong Ignition Limit. Combust. Flame. 17, 65.

Olson, D.B., and Gardiner, W.C. (1977). An Evaluation of Methane Combustion Mechanisms. J. Phys. Chem. 81, 2514.

Oran, E.S. Young, T.R., and Boris, J.P. (1979). Application of Time-Dependent Numerical Methods to the Description of Reactive Shocks. Seventeenth Symposium (International) on Combustion, The Combustion Institute, Pittsburgh, pp. 43-54.

Oran, E.S., and Boris, J.P. (1981a). Detailed Modelling of Combustion Systems. Prog. Energy Combust. Sci. 7, 1.

Oran, E.S., and Boris, J.P. (1981b). Weak and Strong Ignition-II. Naval Research Laboratory Memorandum Repot 4671, Washington, D.C. (also to appear in Combust. Flame).

Oran, E.S., Young, T.R., Boris, J.P., and Cohen, A. (1981a). Weak and Strong Ignition-I. Naval Research Laboratory Memorandum Report 4664, Washington, D.C. (also to appear in Combust. Flame)

Oran, E.S., Boris, J.P., Young, T., Flanigan, M., Burks, T., and Picone, M. (1981b). Numerical Simulations of Detonations in Hydrogen-Air and Methane-Air Mixtures. Eighteenth Symposium (International) on Combustion, The Combustion Institute, Pittsburgh, pp. 1641-1649.

Oran, E.S., Young, T.R. Boris, J.P., and Picone, J.M. (1982). A Study of Detonation Structure: The Formation of Unreacted Gas Pockets. Presented at the Nineteenth Symposium (International) on Combustion, The Combustion Institute, Pittsburgh.

Strehlow, R.A., Crooker, A.J., and Cusy, R.E. (1967). Detonation Initiation Behind an Accelerating Shock Wave. Combust. Flame. 11, 339.

Stull, D.R., and Prophet, H. (Eds.) (1971). JANAF Thermochemical Tables, Nat. Stand. Ref. Data Serv., No. 37, 2nd edition, U.S. National Bureau of Standards, Gaithersburg.

Urtiew, P.A., and Oppenheim, A.K. (1966). Experimental Observations of the Transition to Detonation in an Explosive Gas. Proc. Roy. Soc. A295, 13.

Urtiew, P.A., and Oppenheim, A.K. (1967). Detonative Ignition Induced by Shock Merging. Eleventh Symposium (International) on Combustion, The Combustion Institute, Pittsburgh, pp.665-670.

Williams, F.A. (1965). Combustion Theory, Addison-Wesley, Reading, p. 2.

Young, T.R., and Boris, J.P. (1977). A Numerical Technique for Solving Stiff Ordinary Differential Equations Associated with the Chemical Kinetics of Reactive-Flow Problems. J. Phys. Chem. 81, 2424.

Young, T.R. (1980). CHEMEQ - A Subroutine for Solving Stiff Ordinary Differential Equations. Naval Research Laboratory Memorandum Report 4091, Washington, D.C.

Table I. H_2-O_2 Elementary Reactive Mechanism

Reaction	$k_i = AT^B \exp(-C/T)$[a] A[b]	B	C[b]	References[c]
$H + HO \ddagger O + H_2$	1.40(-14)	1.00	3.50(+03)	[1]
	3.00(-14)	1.00	4.48(+03)	[1]
$H + HO_2 \ddagger H_2 + O_2$	4.20(-11)	0.00	3.50(+02)	[1]
	9.10(-11)	0.00	2.91(+04)	[1]
$H + HO_2 \ddagger HO + HO$	4.20(-10)	0.00	9.50(+02)	[1]
	2.00(-11)	0.00	2.02(+04)	[1]
$H + HO_2 \ddagger O + H_2O$	8.30(-11)	0.00	5.00(+02)	[2]
	1.75(-12)	0.45	2.84(+04)	$k_r = k_f/K_c$
$H + H_2O_2 \ddagger HO_2 + H_2$	2.80(-12)	0.00	1.90(+03)	[1]
	1.20(-12)	0.00	9.40(+03)	[1]
$H + H_2O_2 \ddagger HO + H_2O$	5.28(-10)	0.00	4.50(+03)	[1]
	3.99(-10)	0.00	4.05(+04)	$k_r = k_f/K_c$
$HO + H_2 \ddagger H + H_2O$	1.83(-15)	1.30	1.84(+03)	[3]
	1.79(-14)	1.20	9.61(+03)	[3]
$HO + HO \ddagger H_2 + O_2$	1.09(-13)	0.26	1.47(+04)	$k_f = k_r K_c$
	2.82(-11)	0.00	2.42(+04)	[4]
$HO + HO \ddagger O + H_2O$	1.00(-16)	1.30	0.00(+00)	[3]
	3.20(-15)	1.16	8.77(+03)	$k_r = k_f/K_c$
$HO + HO_2 \ddagger H_2O + O_2$	8.30(-11)	0.00	5.03(+02)	[5]
	2.38(-10)	0.17	3.69(+04)	$k_r = k_f/K_c$
$HO + H_2O \ddagger HO_2 + H_2$	1.70(-11)	0.00	9.10(+02)	[1]
	4.70(-11)	0.00	1.65(+04)	[1]
$HO + H_2 \ddagger HO + H_2O$	1.20(-12)	0.00	9.41(+03)	[4]
	1.33(-14)	0.43	3.62(+04)	$k_r = k_f/K_c$
$HO_2 + HO_2 \ddagger H_2O_2 + O_2^-$	3.00(-11)	0.00	5.00(+02)	[2]
	1.57(-09)	-0.38	2.20(+04)	$k_r = k_f/K_c$

Table I. H_2-O_2 Elementary Reactive Mechanism (Continued)

Reaction	$k_i = AT^B \exp(-C/T)$ [a] A [b]	B	C [b]	References [c]
$O + HO \rightleftarrows H + O_2$	2.72(-12)	0.28	-8.10(+01)	$k_f = k_r K_c$
	3.70(-10)	0.00	8.45(+03)	[1]
$O + HO_2 \rightleftarrows HO + O_2$	8.32(-11)	0.00	5.03(+02)	[5]
	2.20(-11)	0.18	2.82(+04)	$k_r = k_f/K_c$
$O + H_2O_2 \rightleftarrows H_2O + O_2$	1.40(-12)	0.00	2.12(+03)	[2]
	5.70(-14)	0.52	4.48(+04)	$k_r = k_f/K_c$
$O + H_2O_2 \rightleftarrows HO + HO_2$	1.40(-12)	0.00	2.13(+03)	[2]
	2.07(-15)	0.64	8.23(+03)	$k_r = k_f/K_c$
$H + H + M \rightleftarrows H_2 + M$	1.80(-30)	-1.00	0.00(+00)	[1]
	3.70(-10)	0.00	4.83(-04)	[1]
$H + HO + M \rightleftarrows H_2O + M$	6.20(-26)	-2.00	0.00(+00)	[1]
	5.80(-09)	0.00	5.29(+04)	[1]
$H + O_2 + M \rightleftarrows HO_2 + M$	4.14(-33)	0.00	-5.00(+02)	[1]
	3.50(-09)	0.00	2.30(+04)	[1]
$HO + HO + M \rightleftarrows H_2O_2 + M$	2.50(-33)	0.00	-2.55(+03)	[1]
	2.00(-07)	0.00	2.29(+04)	[1]
$O + H + M \rightleftarrows HO + M$	8.28(-29)	-1.00	0.00(+00)	[6]
	2.33(-10)	0.21	5.10(+04)	$k_r = k_f/K_c$
$O + HO + M \rightleftarrows HO_2 + M$	2.80(-31)	0.00	0.00(+00)	[6]
	1.10(-04)	-0.43	3.22(+04)	$k_r = k_f/K_c$
$O + O + M \rightleftarrows O_2 + M$	5.20(-35)	0.00	-9.00(+02)	[1]
	3.00(-06)	-1.00	5.94(+04)	[1]

(a) Bimolecular reaction rate constants are given in units of $cm^3/(molecule\ sec)$. Termolecular reaction rate constants are given in units of $cm^6/(molecule^2\ sec)$.

(b) Exponentials to the base 10 are given in parenthesis; i.e., 1.00(-10) = 1.00×10^{-10}.

(c) The references are: (1) Baulch et al., 1972; (2) Hampson and Garvin, 1975; (3) Cohen and Westberg, 1979; (4) Olson and Gardiner, 1977; (5) Lloyd, 1974; (6) Bahn, 1968.

Table II. Parameters for the Weak Ignition Study.

Parameter	Driver Section	Driven Section
Length	30 cm	370 cm
Gas Mixture	He	$H_2:O_2:N_2/2:1:4$
Initial Temperature	298 K	298 K
Initial Pressure	9 atm	0.1 atm
Incident Shock Velocity		1.4×10^5 cm/s
Temperature behind Incident Shock		918 K
Pressure behind Incident Shock		1.39 atm
Chapman-Jouguet Detonation Velocity		1.9×10^5 cm/s

Table III. Time History of the Forward Moving Reaction Wave.

Time (μs)	Velocity of Wave (cm/s)	Fluid Velocity (cm/s)		Sound Velocity (cm/s)	
		Ahead	Behind	Ahead	Behind
609.03	2.70(+05)	1.09(+05)	1.30(+05)	7.15(+04)	1.10(+05)
618.63	2.72(+05)	1.08(+05)	1.50(+05)	7.15(+04)	1.12(+05)
626.03	2.75(+05)	1.08(+05)	1.60(+05)	7.10(+04)	1.15(+05)
631.83	2.80(+05)	1.08(+05)	1.85(+05)	7.08(+04)	1.14(+05)
663.83	3.20(+05)	1.07(+05)	2.10(+05)	7.20(+04)	1.18(+05)
688.13	2.60(+05)	0	2.10(+05)	4.04(+04)	1.28(+05)

Note: Exponentials to the base 10 are given in parenthesis, i.e., $2.70(+05) = 2.70 \times 10^5$

Table IV. Time History of the Backward Moving Reaction Wave.

Time (μs)	Velocity of Wave (cm/s)	Fluid Velocity (cm/s)		Sound Velocity (cm/s)	
		Ahead	Behind	Ahead	Behind
609.03	-7.2(+04)	1.08(+05)	8.3(+05)	7.2(+04)	1.06(+05)
618.63	-7.3(+04)	1.08(+05)	7.0(+04)	7.2(+04)	1.11(+05)
626.03	-7.5(+04)	1.09(+05)	6.0(+04)	7.2(+04)	1.13(+05)
631.83	-7.6(+04)	1.09(+05)	5.5(+04)	7.2(+04)	1.14(+05)

FIGURE CAPTIONS

Figure 1. A schematic representation of the adaptive grid used for the numerical simulations.

Figure 2. A position-time diagram of the main events occurring in the shock tube simulation: S, incident shock; CS, contact surface; RC, reactive centers, RW, reaction wave; (a) pre-ignition regime, (b) quasi-steady shock-reaction complex, (c) formation of reactive centers, (d) hot spot formation leading to overdriven detonation and (e) detonation relaxation.

Figure 3. The spatial variation of the temperature and the OH mole fraction between the contact surface and the shock at 135 μs.

Figure 4. The spatial distribution of the temperature between the contact surface and the shock at four different times.

Figure 5. The spatial variation of the temperatue and the OH mole fraction between the cntact surface and the shock at (a) 348 μs and (b) 445 μs.

Figure 6. Time history of the development of a hot spot.

Figure 7. A position-time diagram showing the ignition of flamelets and the transition to detonation: A, hot spot and B, flamelets.

Figure 8. The pressure, velocity and temperature distributions across the system at (a) 599.33 μs and (b) 609.03 μs.

Figure 9. The pressure and temperature distributions across the system at (a) 618.63 μs, (b) 626.03 μs and (c) 631.83 μs.

Figure 10. The pressure and temperature distributions across the system at (a) 663.83 μs and (b) 688.13 μs.

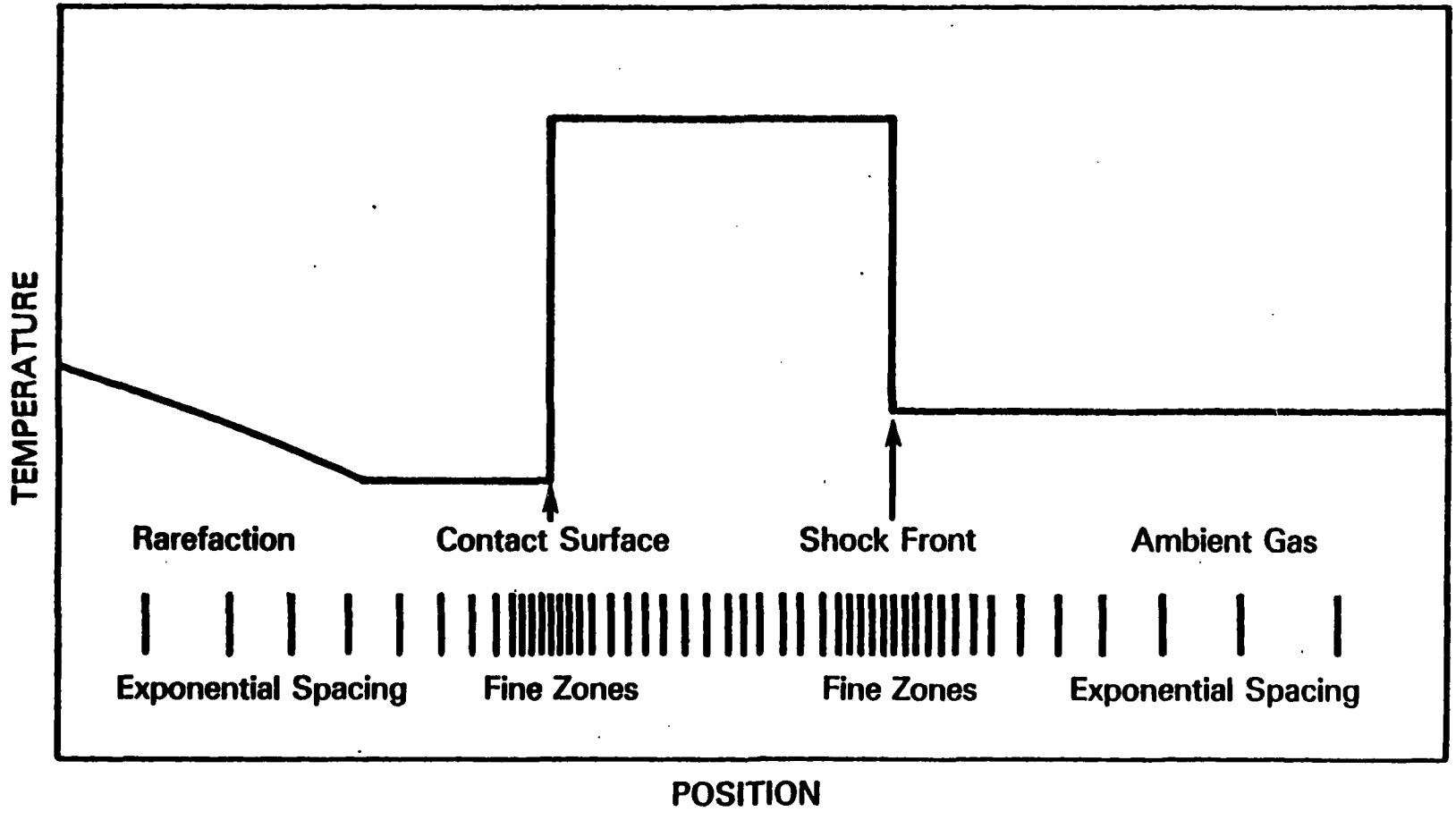
TEMPERATURE
Rarefaction
Contact Surface
Shock Front
Ambient Gas
Exponential Spacing
Fine Zones
Fine Zones
Exponential Spacing
POSITION

Figure 1

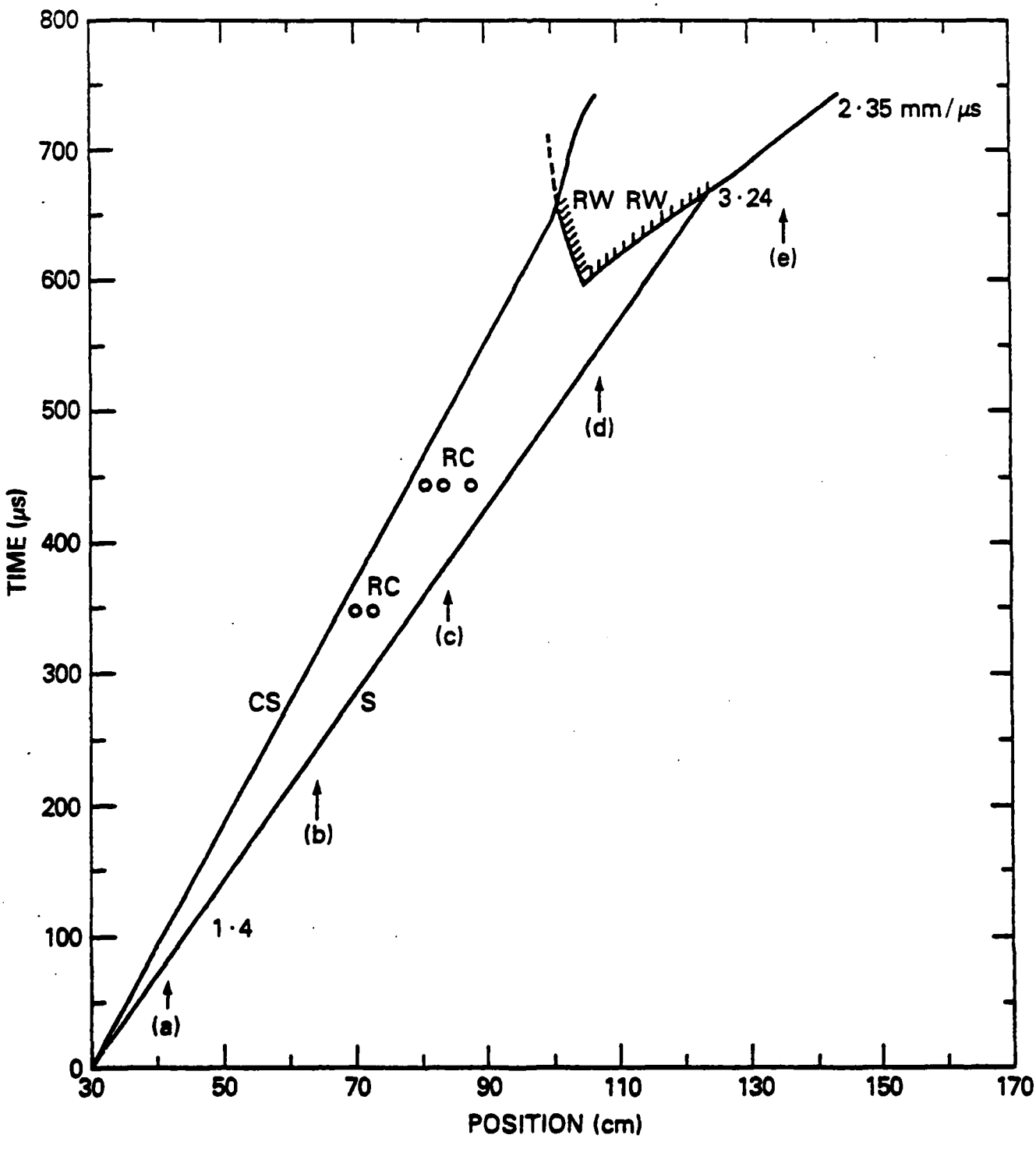
800
700
600
500
400
300
200
100
0
TIME (μs)
30
50
70
90
110
130
150
170
POSITION (cm)
2·35 mm/μs
RW RW
3·24
(e)
(d)
RC
RC
(c)
CS
S
(b)
1·4
(a)

Figure 2

TEMPERATURE (K)
1000
950
850
800
time = 135μs
POSITION (cm)
49
48
47
46
45
44
50
OH MOLE FRACTION x 10^11
16
12
8
4
0

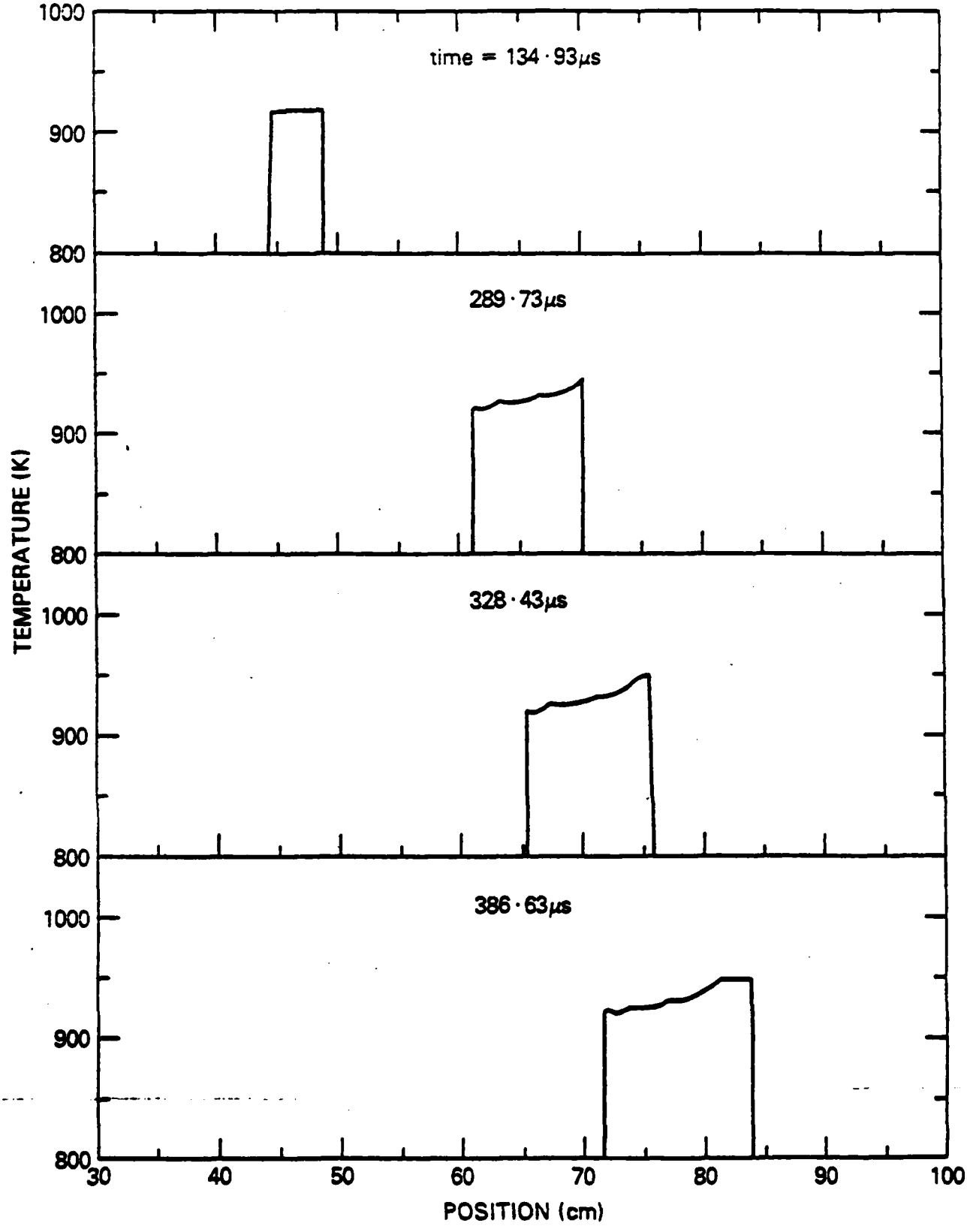
time = 134·93μs
289·73μs
328·43μs
386·63μs
TEMPERATURE (K)
1000
900
800
30
40
50
60
70
80
90
100
POSITION (cm)

Figure 4

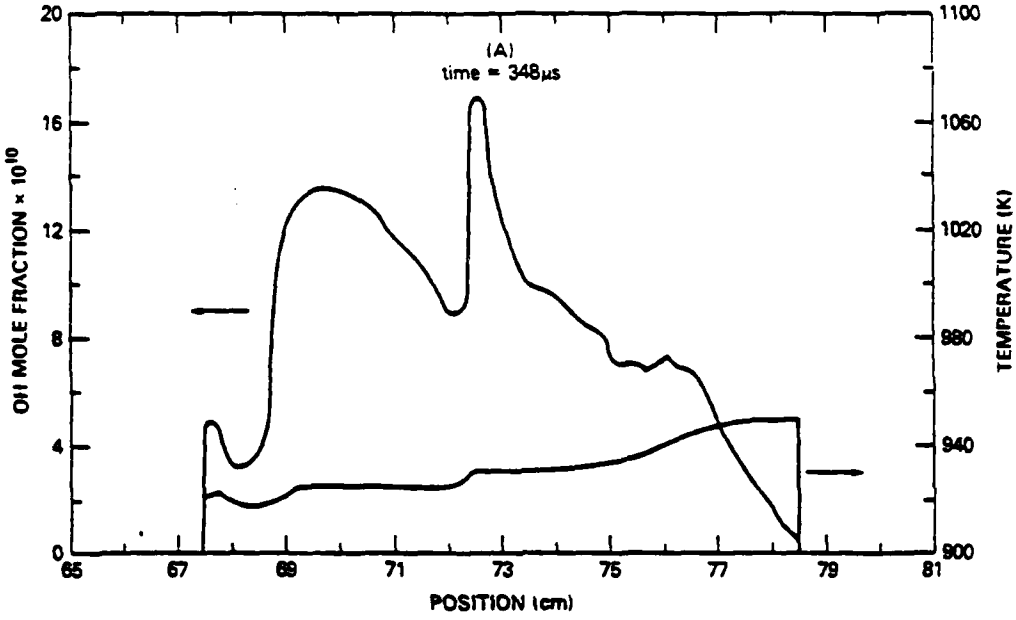
(A)
time = 348μs
OH MOLE FRACTION × 10^10
TEMPERATURE (K)
POSITION (cm)
20
16
12
8
4
0
1100
1060
1020
980
940
900
65
67
69
71
73
75
77
79
81

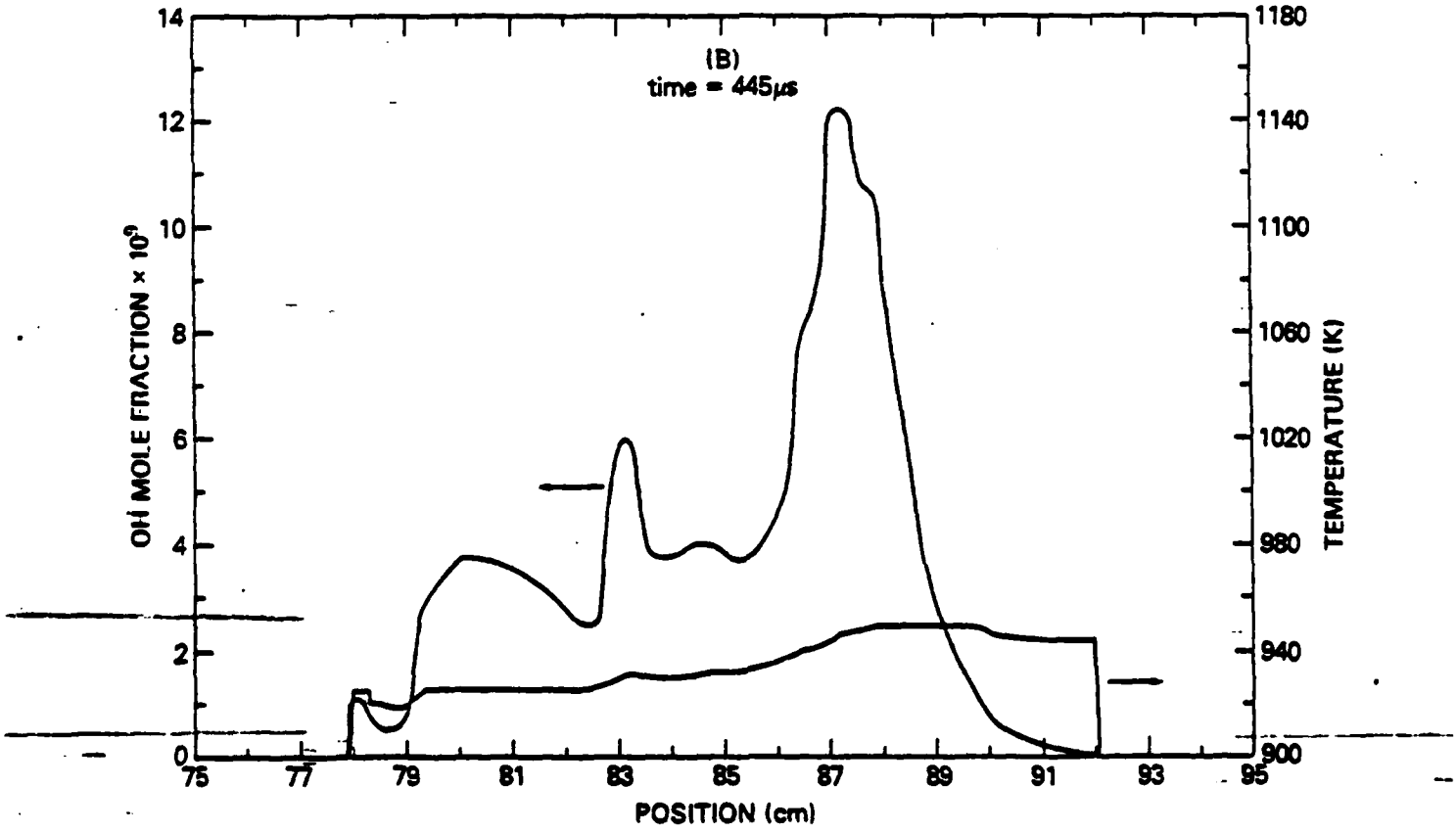
(B)
time = 445μs
OH MOLE FRACTION × 10^9
TEMPERATURE (K)
POSITION (cm)
14
12
10
8
6
4
2
0
1180
1140
1100
1060
1020
980
940
900
75
77
79
81
83
85
87
89
91
93
95

Figure 5

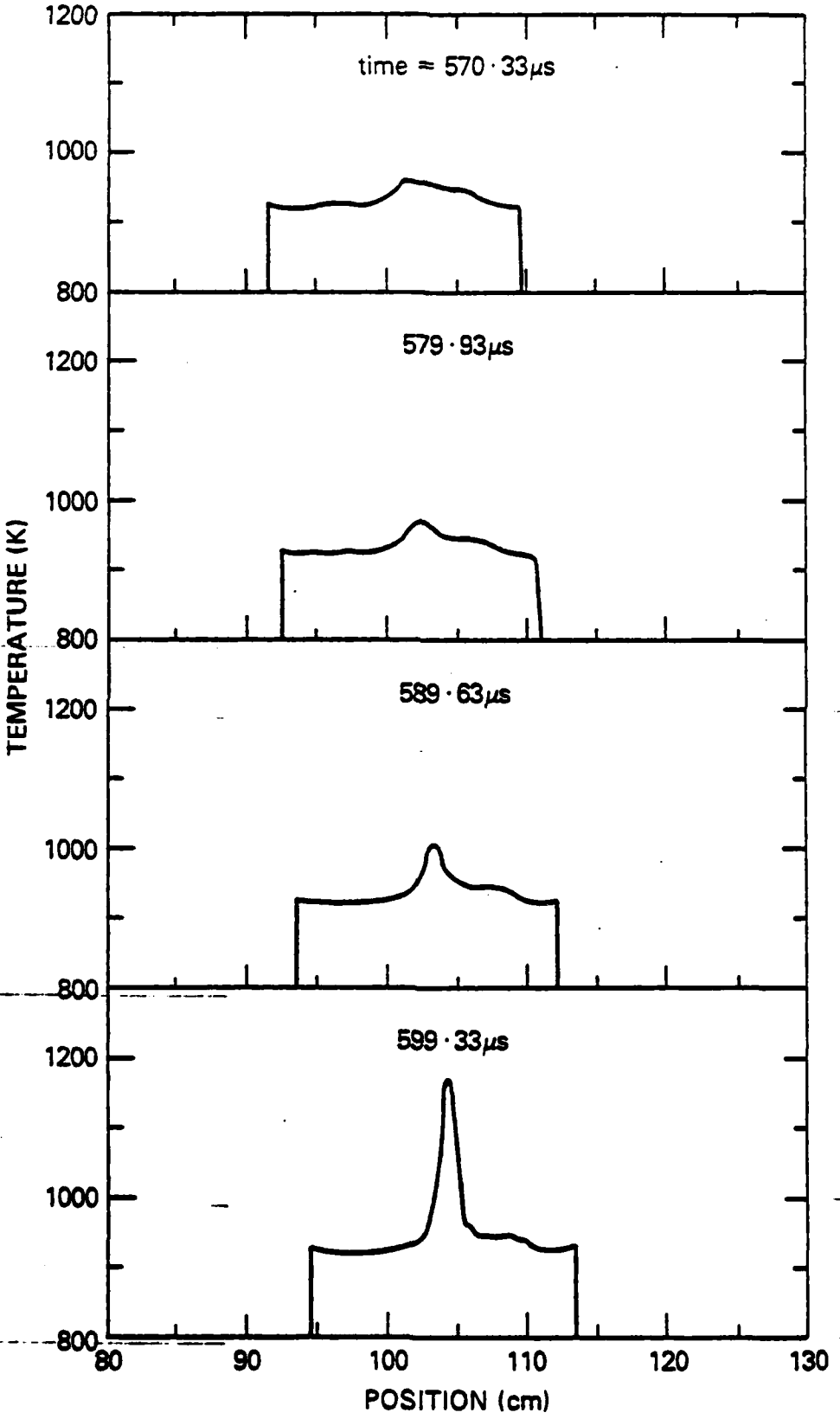
time ≈ 570·33μs
579·93μs
589·63μs
599·33μs
1200
1000
800
TEMPERATURE (K)
80
90
100
110
120
130
POSITION (cm)

Figure 6

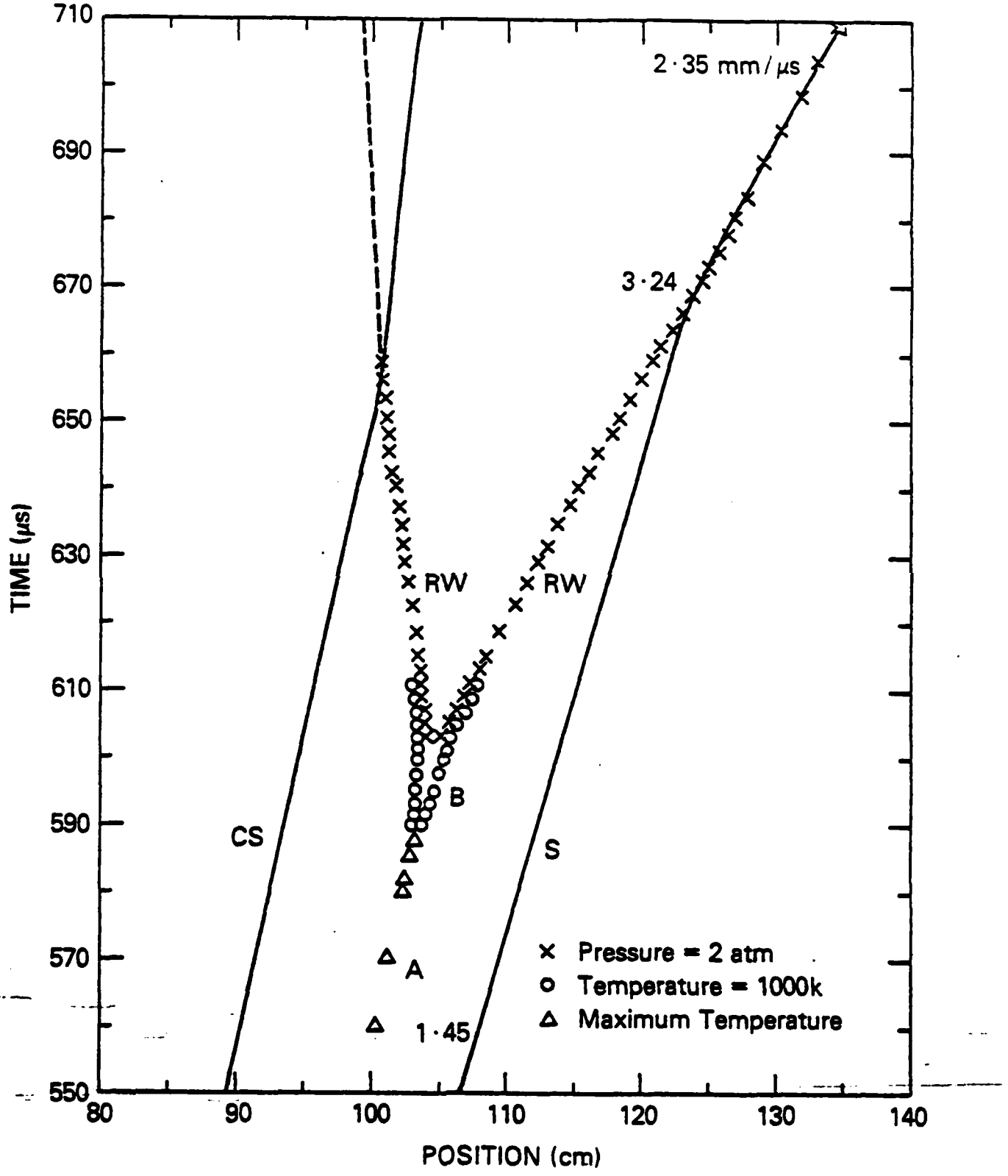
710
690
670
650
630
610
590
570
550
80
90
100
110
120
130
140
TIME (μs)
POSITION (cm)
2·35 mm/μs
3·24
1·45
RW
RW
CS
S
A
B
× Pressure = 2 atm
o Temperature = 1000k
Δ Maximum Temperature

Figure 7

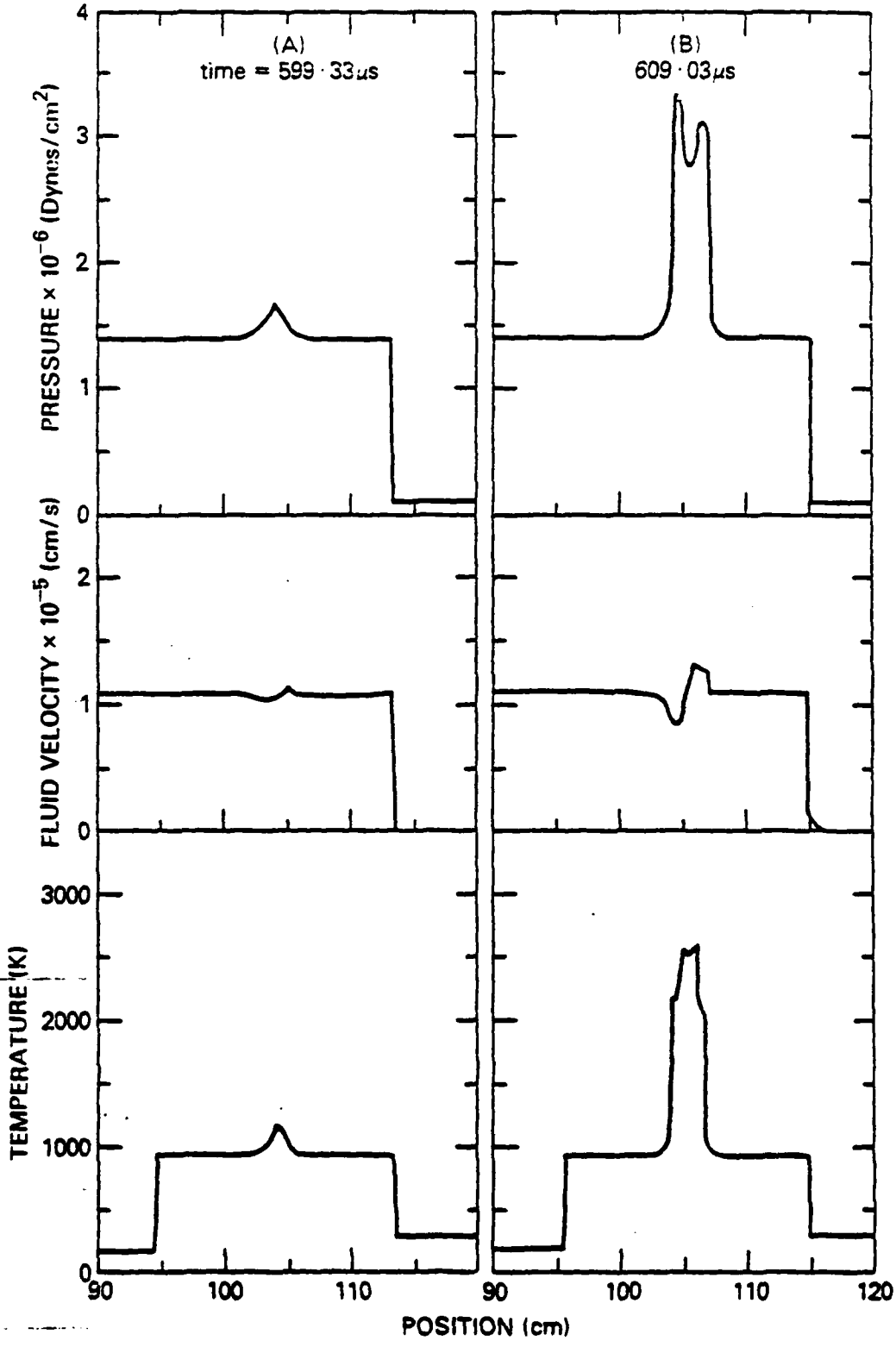
(A)
time = 599·33μs
(B)
609·03μs
PRESSURE × 10⁻⁶ (Dynes/cm²)
FLUID VELOCITY × 10⁻⁵ (cm/s)
TEMPERATURE (K)
POSITION (cm)
0
1
2
3
4
0
1
2
0
1000
2000
3000
90
100
110
90
100
110
120

Figure 8

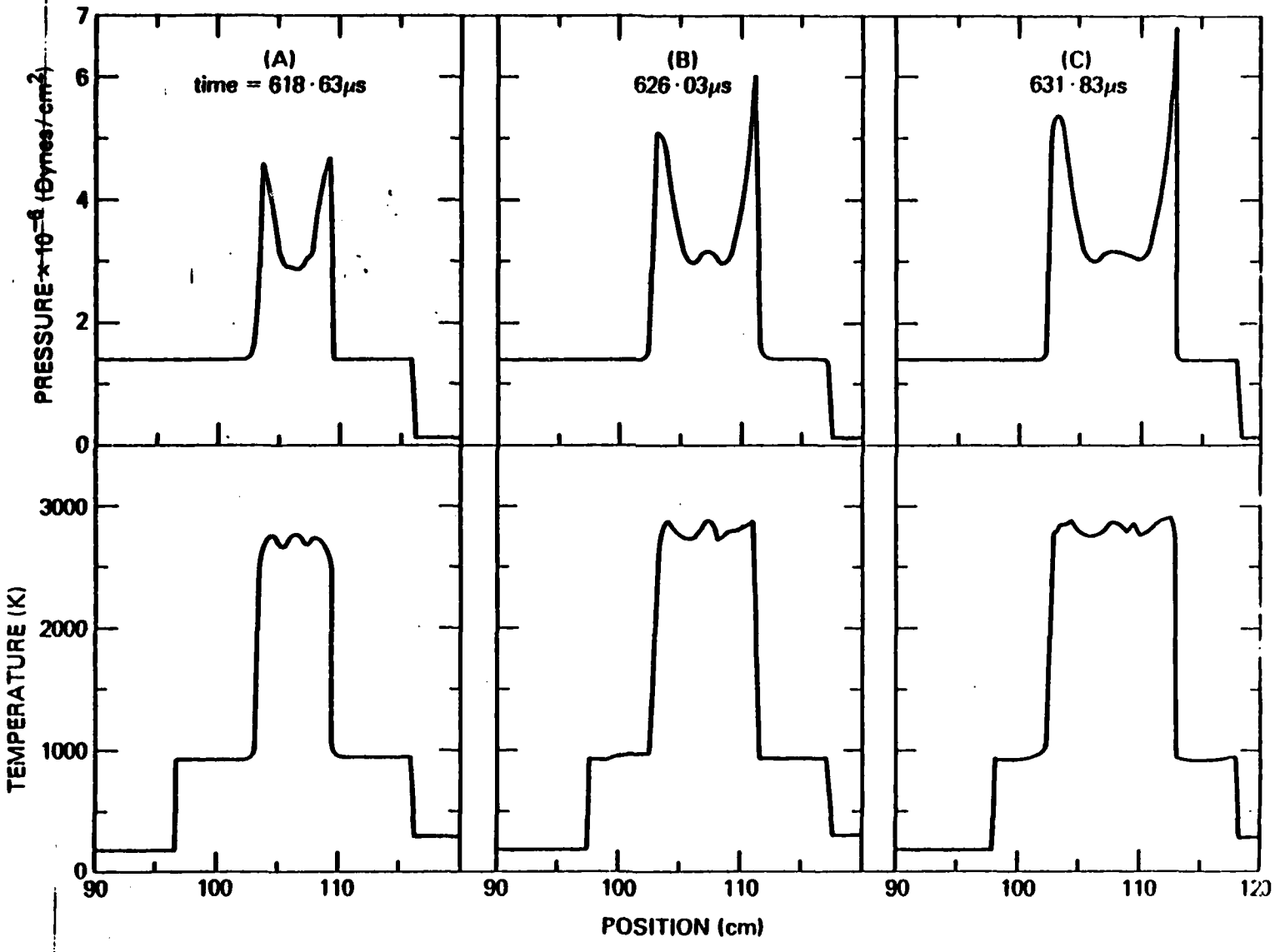
(A)
time = 618·63μs
(B)
626·03μs
(C)
631·83μs
PRESSURE×10⁻⁹ (Dynes/cm²)
TEMPERATURE (K)
POSITION (cm)
0
2
4
6
7
1000
2000
3000
90
100
110
120

Figure 9

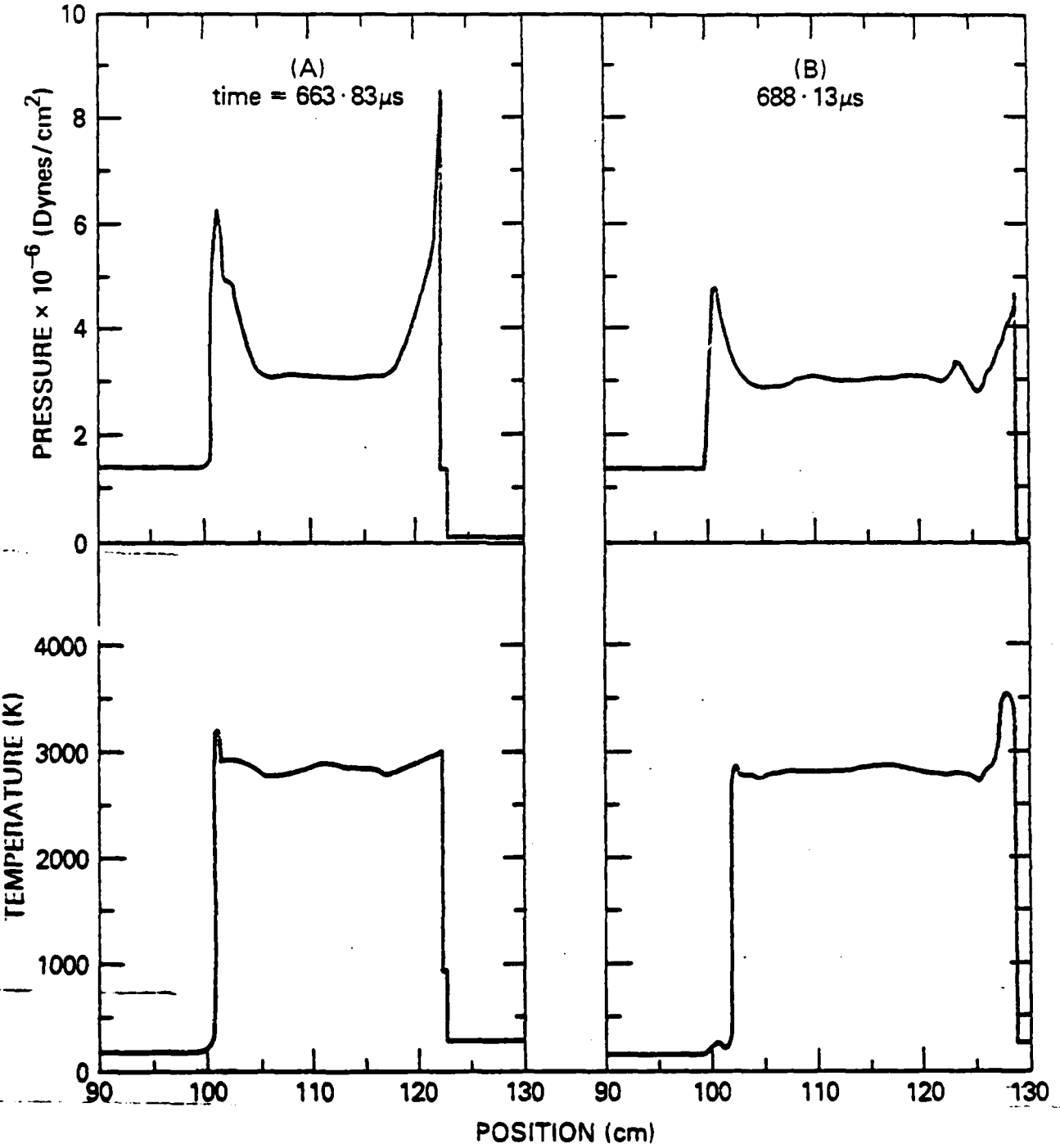
(A)
time = 663·83μs
(B)
688·13μs
PRESSURE × 10⁻⁶ (Dynes/cm²)
TEMPERATURE (K)
POSITION (cm)
0
2
4
6
8
10
1000
2000
3000
4000
90
100
110
120
130

Figure

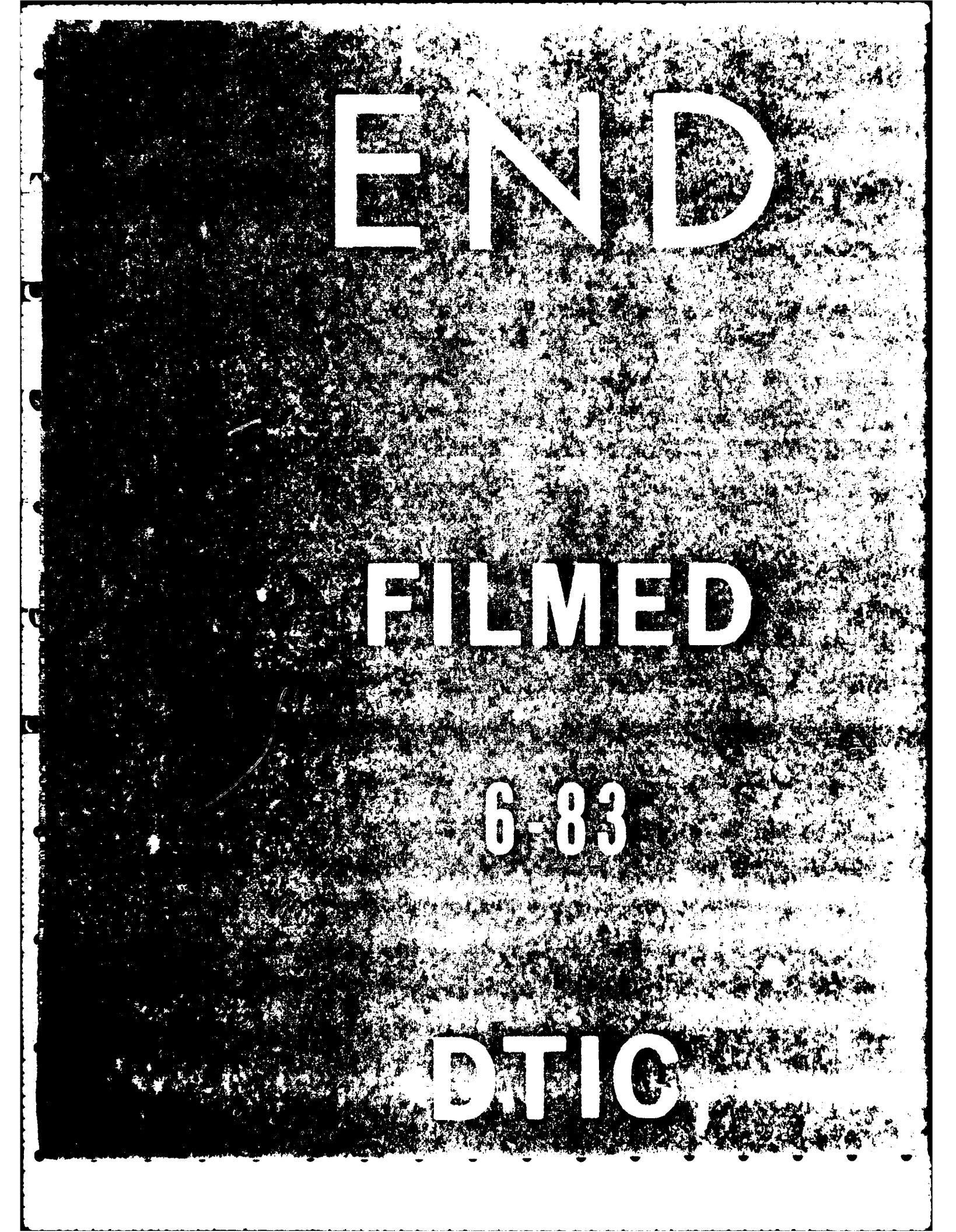
END
FILMED
6-83
DTIC